Atmos. Chem. Phys., 17, 12845–12869, 2017
https://doi.org/10.5194/acp-17-12845-2017

Atmospheric Chemistry and Physics
Open Access
EGU

Vertical distribution of microphysical properties of Arctic springtime low-level mixed-phase clouds over the Greenland and Norwegian seas

Guillaume Mioche[1,2,4], Olivier Jourdan[1,2], Julien Delanoë[3], Christophe Gourbeyre[1,2], Guy Febvre[1,2], Régis Dupuy[1,2], Marie Monier[1,2], Frédéric Szczap[1,2], Alfons Schwarzenboeck[1,2], and Jean-François Gayet[1,2]

[1]Université Clermont Auvergne, OPGC, Laboratoire de Météorologie Physique, 63000 Clermont-Ferrand, France
[2]CNRS, UMR 6016, LaMP/OPGC, BP80026, 63177 Aubière, France
[3]Laboratoire Atmosphère, Milieux et Observations Spatiales, UVSQ/CNRS/UPMC-IPSL, 78035 Guyancourt, France
[4]IUT d'Allier, CS 82235, 03101 Montluçon, France

Correspondence to: Guillaume Mioche (g.mioche@opgc.fr) and Olivier Jourdan (o.jourdan@opgc.fr)

Received: 1 February 2017 – Discussion started: 15 February 2017
Revised: 29 July 2017 – Accepted: 12 September 2017 – Published: 27 October 2017

Abstract. This study aims to characterize the microphysical and optical properties of ice crystals and supercooled liquid droplets within low-level Arctic mixed-phase clouds (MPCs). We compiled and analyzed cloud in situ measurements from four airborne spring campaigns (representing 18 flights and 71 vertical profiles in MPCs) over the Greenland and Norwegian seas mainly in the vicinity of the Svalbard archipelago. Cloud phase discrimination and representative vertical profiles of the number, size, mass and shape of ice crystals and liquid droplets are established. The results show that the liquid phase dominates the upper part of the MPCs. High concentrations (120 cm^{-3} on average) of small droplets (mean values of 15 µm), with an averaged liquid water content (LWC) of 0.2 g m^{-3} are measured at cloud top. The ice phase dominates the microphysical properties in the lower part of the cloud and beneath it in the precipitation region (mean values of 100 µm, 3 L^{-1} and 0.025 g m^{-3} for diameter, particle concentration and ice water content (IWC), respectively). The analysis of the ice crystal morphology shows that the majority of ice particles are irregularly shaped or rimed particles; the prevailing regular habits found are stellars and plates. We hypothesize that riming and diffusional growth processes, including the Wegener–Bergeron–Findeisen (WBF) mechanism, are the main growth mechanisms involved in the observed MPCs. The impact of larger-scale meteorological conditions on the vertical profiles of MPC properties was also investigated. Large values of LWC and high concentration of smaller droplets are possibly linked to polluted situations and air mass origins from the south, which can lead to very low values of ice crystal size and IWC. On the contrary, clean situations with low temperatures exhibit larger values of ice crystal size and IWC. Several parameterizations relevant for remote sensing or modeling studies are also determined, such as IWC (and LWC) – extinction relationship, ice and liquid integrated water paths, ice concentration and liquid water fraction according to temperature.

1 Introduction

The Arctic region is more sensitive to climate change than any other region of the Earth (Solomon et al., 2007). Clouds and particularly low-level mixed-phase clouds related processes have a major impact on the Arctic surface energy budget (Curry, 1995; Curry et al., 1996; Morrison et al., 2012). Observations suggest that boundary layer mixed-phase clouds (MPCs, mixture of liquid droplets and ice) are ubiquitous in the Arctic and persist for several days under a variety of meteorological conditions (Mioche et al., 2015; Morrison et al., 2012; Shupe et al., 2011; Shupe and Intrieri, 2004). They occur as single or multiple stratiform layers of supercooled droplets near the cloud top in which ice crystals can form and precipitate. These clouds have a large impact on the surface radiative fluxes and Arctic climate feedbacks

(Kay et al., 2012; Kay and Gettelman, 2009). The strong impact of MPCs on the energy budget stems from their persistence and microphysical properties which result from a complex web of interactions between numerous local and larger-scale processes that greatly complicate their understanding and modeling (Klein et al., 2009; Morrison et al., 2012).

However, major uncertainties limit our understanding of the interactions and feedbacks between the physical processes involved in their life cycle. This complexity translates into the large discrepancies that can be found in numerical models to represent the cloud processes, which in turn impacts their capability to forecast cloud properties in the Arctic. For instance, global climate models (GCMs) tend to underestimate the amount of liquid water in MPCs (Komurcu et al., 2014). Therefore, the representation of ice formation and growth processes and their interactions with the liquid phase (e.g., liquid/ice partitioning, Wegener–Bergeron–Findeisen process) has to be improved, as already shown in previous modeling studies (Prenni et al., 2007 or Klein et al., 2009). Among the various cloud properties which need to be described more accurately, the cloud thermodynamic phase is a parameter of primary importance since it governs the cloud optical and therefore radiative properties as well as its life cycle (longevity and precipitation formation).

However, measuring the spatial phase distribution in low-level Arctic mixed-phase clouds, in order to relate it to environmental conditions (height, temperature, surface conditions, air mass origins, etc.) to parameterize and model it, remains a challenge. The parameterizations of liquid and ice partitioning in numerical simulations vary from one model to another. A study carried out by Klein et al. (2009) compared outputs from 26 different numerical models. They found that using different schemes of temperature-dependent partitioning yields liquid water content ranging from 12 to 83 % for the same cloud top temperature of $-15\,^{\circ}\mathrm{C}$.

Beyond the experimental limitations related to the accurate measurement of the phase partitioning (discussed hereafter), the cloud phase quantification is also hampered by difficulties to translate observational characterization into realistic representations for cloud models with a wide range of scales. The definition of a mixed-phase system is actually controversial. A mixed-phase cloud can be regarded as a complete cloud system that contains both liquid and ice involved in mixed microphysical processes but does not necessarily imply that all volumes in the system contain both phases (Shupe et al., 2008). Additionally, the definition of a mixed-phase cloud or volume could be based either on a threshold value for its optical properties or for the ratio between supercooled liquid droplets and ice crystal mass or number (Cober et al., 2001). The threshold values are questionable. The standard assumption in climate models is that liquid and ice are uniformly mixed throughout each entire model grid box (with a typical horizontal resolution of 100 and 1 km in the vertical; Tan and Storelvmo, 2016). However, some field measurements (see, among others, Rangno and Hobbs, 2001 or Korolev and Isaac, 2003) suggest that different pockets of solely water or ice in mixed-phase regions coexist with typical scale of tens of meters. This has consequences on how processes like the Wegener–Bergeron–Findeisen process (WBF, Bergeron, 1935; Findeisen, 1938; Wegener, 1911) should be parameterized in large-scale models.

A better assessment of the ice/liquid partitioning will improve our understanding of the life cycle and more precisely the persistence of MPCs since modeling studies show that this persistence is governed by a delicate balance between dynamical, radiative and microphysical processes occurring mainly in the boundary layer (Savre and Ekman, 2015). This understanding is still limited by the description of the microphysical processes related to the initiation and the maintenance of the ice phase. The cloud processes responsible for the production of ice crystals in the upper part of the cloud seem to be mostly driven by the cloud top temperature and the entrainment rates (Savre and Ekman, 2015). In particular, the assessment of ice nuclei (IN) concentration and its time evolution is of primary importance but relies on a very limited set of in situ observations and needs to be improved (Ovchinnikov et al., 2014). The ice crystal number concentrations usually exceed the number of IN particles. These discrepancies could be explained by the limitations of in situ instruments and especially the overestimation of the ice crystal number due to the shattering of large ice crystals on the probe inlets or the inability of instruments measuring IN particles to detect all the activation modes (Baumgardner et al., 2012; Korolev et al., 2011). Secondary ice formation processes or the recycling of IN particles through subcloud sublimation (Lawson et al., 2001; Rangno and Hobbs, 2001; Solomon et al., 2015) may also play an important role and explain such discrepancies. Given the temperatures observed in MPCs, heterogeneous ice nucleation mechanisms are preferentially involved. The concentration of large ice crystals ($> 100\,\mu\mathrm{m}$) in particular may be due to heterogeneous ice formation mechanisms (Eidhammer et al., 2010; Prenni et al., 2009). However, which process (among deposition, condensation, immersion or contact freezing processes) is mainly responsible for the initiation of ice crystals is still under debate, as modeling studies fail to reproduce the observed ice number concentration (Avramov and Harrington, 2010; Fridlind et al., 2007). In a recent modeling study linked to the Aerosol-Cloud Coupling and Climate Interactions in the Arctic (ACCACIA) campaign, Young et al. (2017) showed that small differences in the predicted ice concentration can have large effects on the microphysical structure (such as ice/liquid partitioning) and lifetime of single-layer MPCs. They suggested that the method of parameterizing primary ice concentration in bulk microphysical models is therefore of primary importance.

The recent developments of ground-based stations (Barrow, EUREKA, Ny-Ålesund, among others) and spaceborne remote sensing observations (as lidar and radar observations from the CALIPSO and CloudSat platforms, respectively)

allow reliable studies today of Arctic cloud phase variability from a few kilometers to the pan-Arctic region (Dong et al., 2010; Kay and Gettelman, 2009; Liu et al., 2012; Shupe et al., 2011). Moreover, remote sensing observations from space performed by active instruments onboard CALIPSO (Winker et al., 2003) and CloudSat (Stephens et al., 2002) satellites as a part of the A-Train constellation provide a unique way of characterizing Arctic cloud vertical properties. However, the cloud phase distribution and characterization are highly dependent on the measurement principle of the instruments.

The aforementioned techniques provide cloud properties typically averaged over 1 km, which may be insufficient to study cloud processes at a microphysical scale (i.e., measurements of microphysical cloud properties, spatial resolution less or equal to 100 m). In situ observations are based on direct measurement techniques at a higher spatial resolution (generally < 100 m). Numerous previous studies dedicated to the assessment of the in situ microphysical properties of Arctic clouds focused on specific case studies (Avramov et al., 2011; Gayet et al., 2009; Rangno and Hobbs, 2001; Verlinde et al., 2007). Statistical analysis of mixed-phase cloud properties derived from several in situ datasets or airborne campaigns are very scarce and often focus on the western Arctic region (McFarquhar et al., 2007; Jackson et al., 2012). Such data analysis strategy is still missing in the European Arctic region (and in the vicinity of Svalbard, over the Greenland and Norwegian seas in particular).

In Mioche et al. (2015), the spatial, seasonal and surface conditions' variability of MPC properties using CloudSat and CALIPSO spaceborne observations has been investigated. The study showed a large occurrence of MPCs all year long both over the whole Arctic and the Svalbard regions. It was clearly evidenced that the Svalbard region, due to its specific location near the Atlantic Ocean, presents a larger occurrence of low-level MPCs compared to the averaged Arctic. Then, it appears important to investigate the microphysical properties of MPCs in the Svalbard and Greenland Sea regions from a statistical point of view to provide representative profiles that can be compared to previous works focused on the western Arctic region.

This work provides statistical analysis of liquid and ice properties of low-level Arctic MPCs from in situ data collected in single-layer MPCs during several airborne campaigns in the region of Norwegian and Greenland seas carried out between 2004 and 2010. We compiled observations of microphysical composition of Arctic mixed-phase clouds (cloud phase, hydrometeor number, mass and shape) to present vertical profiles of liquid and ice properties. The main objective is a step to a better understanding of the processes involved in the Arctic low-level MPC life cycle at the microphysical scale. We aimed to relate these properties to environmental conditions in order to improve the cloud parameterizations used in models and remote sensing algorithms. The results will also complement previous works concerning Arctic cloud characterizations performed in the western Arctic.

This paper is organized in four sections. The description of the field experiments, instrumentation and datasets will be made in Sect. 2. Section 3 will present and discuss the vertical profiles of microphysical properties of the low-level MPCs. Finally, key parameterizations useful for modeling or remote sensing will be proposed in Sect. 4.

2 Field experiments, airborne measurements and meteorological situations

2.1 Airborne campaigns

This study is based on in situ data collected in single-layer MPCs during the following four international airborne campaigns organized in the "European" Arctic region:

i./ii. The Arctic Study of Tropospheric Aerosols, clouds and Radiation experiments (ASTAR; Herber et al., 2004; Jourdan et al., 2010; Ehrlich et al., 2009; Gayet et al., 2009; Lampert et al., 2009) took place in the vicinity of Svalbard (Longyearbyen, Norway, 78° N, 15° E) in April 2004 and April 2007. The Polar-2 aircraft operated by AWI (Alfred Wegener Institute) was flown during these two experiments.

iii. The Polar Study using Aircraft, Remote Sensing, Surface Measurements and Models, of Climate, Chemistry, Aerosols, and Transport (POLARCAT-France; Delanoë et al., 2013; Law et al., 2008; Quennehen et al., 2011) was carried out in northern Sweden (Kiruna, 68° N, 20° E) in April 2008 during the International Polar Year. Measurements were performed onboard the French ATR-42 aircraft of SAFIRE (Service des Avions Français Instrumentés pour la Recherche en Environnement).

iv. The Solar Radiation and Phase Discrimination of Arctic Clouds experiment (SORPIC; Bierwirth et al., 2013) was performed in the Svalbard region in May 2010 with the AWI Polar-5 aircraft.

All the clouds sampled during these four campaigns were located over the Arctic Greenland and Norwegian seas as displayed in Fig. 1. The scientific flights during ASTAR and SORPIC covered latitudes ranging from 75 to 79° N (Greenland Sea) while the flights during POLARCAT were performed between 70 and 73° N (Norwegian Sea). Moreover, the data were all collected during spring (April and May).

For this study, we restricted the measurements to continuous ascent and descent flight sequences into single-layer MPCs at the aircraft speed (between 80 and 100 m s^{-1} for all campaigns) since our main objective is to study the vertical partitioning of ice and liquid thermodynamical phases. Our

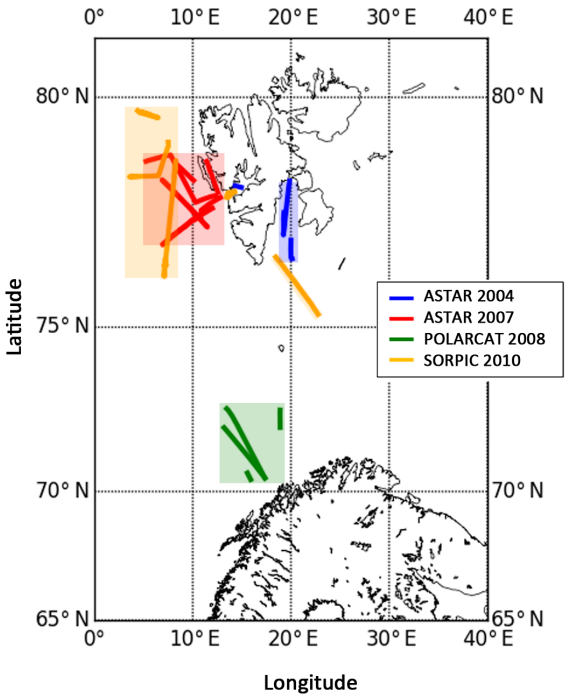

Figure 1. Location of the MPC measurements during the ASTAR, POLARCAT and SORPIC campaigns.

dataset consists of 71 cloud profiles (see Table 1) representing more than 21 000 measurement points at 1 Hz (350 min of cloud observations), spread out over 18 flights performed above Arctic open sea water.

2.2 In situ instrumentation

A similar in situ instrumentation was loaded on the three aircraft: the German Polar-2 and Polar-5 and the French ATR-42. The same data processing procedure was used in order to derive the cloud microphysical parameters (at the same scale: i.e., $\sim$ 100 m). This consistent cloud dataset is used to achieve a statistically representative description of the properties of Arctic mixed-phase clouds sampled over the Greenland and Norwegian seas during spring.

The suite of in situ instruments used to measure the MPC microphysical and optical properties consists of the following:

- The cloud particle imager (CPI; Lawson et al., 2001) captures cloud particle images on a 1024 $\times$ 1024 pixel CCD camera with a pixel resolution of 2.3 µm and 256 grey levels. At least 5 pixels are necessary to identify a cloud particle, so the particle sizes derived from the CPI range from 15 µm to approximately 2 mm. The images are processed using the software developed at the Laboratoire de Météorologie Physique (LaMP; Lefèvre, 2007) based on the original CPIView software (Lawson et al., 2001; Baker and Lawson, 2006). In particular, it provides particle size distribution (PSD) and derived microphysical parameters such as particle concentration, effective diameter, extinction coefficient and ice water content as well as a particle habit classification. The data processing method used to derive the extinction coefficient (σ) and the ice water content (IWC) is described in Appendix A.

- The forward scattering spectrometer probe (FSSP-100; Baumgardner et al., 2002; Knollenberg, 1981) provides the droplet size distribution from 3 to 45 µm. The derived parameters from the PSD are the droplet concentration, the effective diameter, the extinction coefficient (σ) and the liquid water content (LWC).

- The polar nephelometer (PN; Gayet et al., 1997) measures the angular scattering intensities (non-normalized scattering phase function) of an ensemble of cloud particles (either droplets, ice crystals or a mix), from a few micrometers to about 800 µm. In particular, these measurements are used to distinguish spherical from non-spherical particles and thus discriminate the dominant cloud thermodynamical phase. The extinction coefficient and the asymmetry parameter (g) are calculated following the methodology presented in Gerber et al. (2000) and Gayet et al. (2002).

- The Nevzorov probe (Korolev et al., 1998) uses the hot-wire technique to retrieve the liquid water content and the total water content. Note that the Nevzorov data are only used to determine liquid water content during ASTAR 2004 because the FSSP-100 was not used during this campaign. The retrieval method used to determine the liquid water content is described in Appendix A.

All these cloud probes were heated in order to avoid icing during the flights. The combination of these probes provides the microphysical properties of cloud particles from a few micrometers (typically 3 µm) to about 2 mm. Data are recorded at 1 Hz frequency, which corresponds to a spatial resolution of about 100 m (according to the aircraft speed). The uncertainties and measurement ranges associated with the derived cloud parameters are summarized in Table 2. However, it should be noted that in situ measurements' accuracy may be hampered by the shattering of large ice crystals on the probe inlets, inducing smaller particle artifact (Heymsfield, 2007), leading to an overestimation of small particle concentration. For example, previous studies of Field et al. (2003) and Heymsfield (2007) showed that the shattering effect may lead to an overestimation of about 20 % on the bulk properties and a factor 2 or 3 on the number concentration of ice crystals. Moreover, the recent study by Guyot et al. (2015) that compared in situ measurements with the same probes and similar inlet design in a wind tunnel experiment showed that measured particles can vary from one instrument to another and careful calibration is needed. Even through no

Table 1. Summary of in situ observations of Arctic single-layer MPCs.

Field experiment	Location (latitude range)	Date	Number of flights in MPCs	Number of profiles in MPCs	Duration of data (min)
ASTAR 2004	Spitsbergen (Norway) 76–79° N	May 2004	4	7	30
ASTAR 2007	Spitsbergen (Norway) 76–79° N	April 2007	5	34	173
POLARCAT 2008	Kiruna (Sweden) 68–73° N	April 2008	4	10	45
SORPIC 2010	Spitsbergen (Norway) 75–78° N	May 2010	5	20	109
Total			18	71	357

standard method was available during the campaigns to accurately determine and remove the impact of the shattering (designed tips, particle interarrival time measurement, etc.), a short analysis is described in Appendix B for the control of the data quality and the significance of the shattering effect. Comparing the extinction coefficient measured by the PN measurements to the extinction derived from the combination of the CPI and FSSP measurements showed that the shattering effect, in our case, was smaller than the measurement uncertainties (i.e., 25, 35 and 55 % for PN, FSSP and CPI, respectively; see Table 2).

The three research aircraft also measured basic meteorological parameters along the flight track (see Gayet et al., 2009). We recall that the static air temperature is calculated with an accuracy better than ± 0.5 K. If high liquid water contents can alter these temperature measurements, the observed contents, lower than $0.6\,\mathrm{g\,m^{-3}}$ during most of the MPC flights, ensure that this effect was not significant along the cloud transects. The altitude and geographical position parameters were measured by the airborne GPS systems with an accuracy of 50 m.

2.3 Normalized altitudes

Table 3 summarizes, for the 71 selected profiles, the statistics of altitudes for the MPCs' top and base, as well as the thickness of the cloud layer containing liquid water. The mean cloud top altitude is located around 1200 ± 310 m, while the mean cloud base altitude (referring to the altitude below which liquid phase is no longer present) is 756 ± 283 m. This is consistent with observations performed in the western Arctic where cloud top altitudes lie between 885 and 1320 m, and cloud base altitudes between 420 and 745 m (McFarquhar et al., 2007). Our measurements also indicate that the thickness of the liquid layer spans from 100 to 950 m with an averaged value of 444 m. The objective of this study is to merge and analyze the MPC microphysical data obtained during the four airborne campaigns to derive representative vertical profiles. Since cloud top and cloud base heights exhibit large variability (see Table 3), the altitudes are normalized following the method presented in Jackson et al. (2012). The cloud top and cloud base refer to the liquid phase layer, i.e., the cloud layers containing liquid droplets (mixed-phase or liquid only). These layers are identified based on the PN asymmetry parameter values greater than 0.8 (Jourdan et al., 2010; see Sect. 2.4 below). Within these layers (Eq. 1) and below the cloud base (Eq. 2) the normalized altitudes Z_n are defined as follows:

$$Z_\mathrm{n} = \frac{Z - Z_\mathrm{b}}{Z_\mathrm{t} - Z_\mathrm{b}} \quad \text{for } z_\mathrm{b} < z < z_\mathrm{t} \tag{1}$$

$$Z_\mathrm{n} = \frac{Z}{Z_\mathrm{b}} - 1 \quad \text{for } z < z_\mathrm{b}, \tag{2}$$

where Z_n is the normalized altitude, Z the altitude corresponding to the aircraft measurements, and Z_t and Z_b the cloud top and base altitudes, respectively. Thus, an altitude of 1 corresponds to the top-of-the-cloud liquid-containing layer and 0 to its base. Negative values characterize regions of ice precipitation below the cloud layer and the altitude of -1 defines the ground level according to Eq. (2).

To obtain representative statistical results, the cloud layers have been stratified in 10 levels with intervals of 0.2 of normalized altitude, each containing around 2000 observations (i.e., about 10 % of the dataset). The vertical profiles of MPC microphysical properties presented hereafter are obtained by averaging the in situ measurements over each normalized altitude layer. The profiles are computed for the whole dataset and for each main meteorology situation separately (see Sect. 2.5) for a better analysis and discussions of the results.

2.4 Determination of the cloud thermodynamical phase from in situ measurements

As stated above, the asymmetry parameter (g) derived from the PN scattering phase function (PhF) measurements is used to discriminate cloud thermodynamic phase. Indeed, in a previous study, Jourdan et al. (2010) have shown with a principal component analysis that g is a reliable proxy to determine the cloud phase of Arctic MPCs. One can notice that our phase discrimination is considered from an optical point of view and differs from the one used by Korolev et al. (2003) which is based on the ice water fraction (IWC/TWC) to identify cloud phase. Large values of g (> 0.83) are typical of an ensemble of particles optically dominated by liquid water droplets where ice crystals do not significantly affect the optical properties. On the contrary, smaller values of g (< 0.80)

Table 2. Uncertainties of cloud properties derived from CPI, FSSP, PN and Nevzorov instruments.

Probe (measurements range)	Number concentration (N)	Extinction coefficient (σ)	Effective diameter (D_{eff})	Water contents (IWC or LWC)	Asymmetry parameter (g)
CPI (15 µm to 2.3 mm)	50 %	55 %	80 %	60 %	–
FSSP-100 (3 to 45 µm)	10 %	35 %	4 %	20 %	–
PN (< 800 µm)	–	25 %	–	–	4 %
Nevzorov (LWC > 0.003–0.005 g m^{-3})	–	–	–	20 %	–

Table 3. Statistics of cloud base and cloud top altitudes along with cloud layer thickness obtained from the 71 profiles sampled in MPCs.

	Mean	SD	Median	25th percentile	75th percentile	Max.	Min.
z_{top} (m)	1200	310	1200	1000	1370	2120	525
z_{base} (m)	756	283	700	510	850	1700	400
Layer thickness (m)	444	211	420	270	600	950	100

are characteristic of a cloud optically dominated by ice crystals, with negligible contribution of liquid droplets. For g ranging from 0.80 to 0.83, both liquid droplets and ice crystals contribute to the optical properties. The optical signature of the ice is more pronounced (i.e., g decreases) as the concentration and/or the size of ice particles become larger. These results are well illustrated and discussed by Febvre et al. (2012) where PN measurements were combined with FSSP and CPI data.

Figure 2 displays the mean PN scattering phase function (Fig. 2a) according to the normalized MPC altitude levels as well as the vertical profile of the corresponding g values (Fig. 2b). At cloud top, the PhF is characterized by rather high scattering at forward angles (angles lower than 60°) associated with lower scattering at sideward angles (60–130°) and enhanced scattering around 140°. These features are representative of cloud layers dominated by spherical particles (mainly supercooled liquid droplets), corresponding to typical g values greater than 0.83. As Z_{n} decreases, the PhF becomes smoother and more featureless. A side scattering enhancement is observed along with an attenuation of the 140° peak. This behavior can be attributed to the presence of nonspherical ice crystals increasing towards the cloud base. This is in agreement with the continuous decrease of g values observed from cloud top (0.84) to cloud base (0.82). Figure 2 also shows that the ice phase region below the cloud layer ($-1 < Z_{\text{n}} < 0$) is characterized by a featureless and flat (at side scattering angles) PhF, with no significant influence of the altitude. These PhF shapes are associated with g values smaller than 0.8. It is thus clearly shown that the PhF and asymmetry parameter are related to specific microphysical properties encountered at different cloud levels. These observations demonstrate that the PhF and the asymmetry parameter can be regarded as an accurate signature of the main microphysical properties observed in the MPC layer particles.

The liquid droplet properties are determined from the FSSP or Nevzorov probe measurements when g values are greater than 0.8 (i.e., indicating a "liquid-containing" phase). Accordingly, the ice crystal properties are derived from CPI measurements when g values are lower than 0.83 (i.e., indicating an "ice-containing" phase). For g ranging between 0.8 and 0.83, both liquid and ice properties are derived. Moreover, CPI particle images classified as spherical droplets are not taken into account for the determination of ice crystal microphysical parameters. Table 4 summarizes the cloud phase analysis.

2.5 Meteorological situations

All the selected situations correspond to low-level single-layer mixed-phase clouds in the boundary layer during spring. If these criteria ensure the homogeneity of the dataset, weather conditions still vary significantly from one campaign to another or even within a campaign. In order to provide a comprehensive dataset to improve model parameterization, it is of great importance to discriminate and classify the observations depending on environmental conditions. The most trivial classification is the temperature regime. Savre and Ekman (2015), showed that it is one of the major factors (with cloud top entrainment) controlling the production of new ice crystals and the maintenance of MPCs. In the present study, two temperature regimes have been selected based on the mean cloud top temperature of each situation: the "cold" situations ($-22\,°\text{C} < T_{\text{Top}} < -15\,°\text{C}$) and the "warm" situations ($-15\,°\text{C} < T_{\text{Top}} < -8\,°\text{C}$). In spring, the cold polar vortex that covers the Arctic region weakens and inclusions of midlatitude air masses are more likely. Atmospheric properties such as temperature, humidity and particle loading can change significantly. Arctic cloud properties are then strongly linked to the air mass origin (Gultepe et al., 2000; Gultepe and Isaac, 2002), since their formation is driven by the aerosol particle properties and thermodynami-

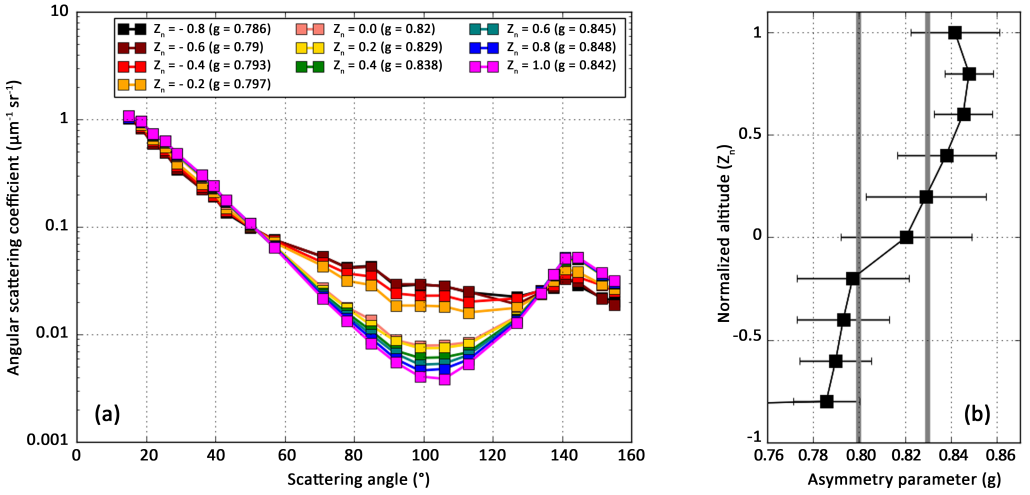

Figure 2. **(a)** Normalized scattering phase function according to the normalized altitude from polar nephelometer measurements (few µm to around 800 µm size range), averaged over all the campaigns. g values indicate the cloud phase: $g < 0.80$: ice; $0.80 < g < 0.83$: mixed; and $g > 0.83$: liquid. **(b)** Mean vertical profile of asymmetry parameter (for all the campaigns). The grey bars indicate the threshold g values for the assessment of ice, mixed and liquid cloud phases.

Table 4. Summary of the method for the assessment of the cloud thermodynamical phase and liquid droplet and ice crystal properties from the combination of PN, CPI, FSSP and Nevzorov probes.

	PN g values (corresponding cloud phase)		
	$g < 0.80$ (ice)	$0.80 < g < 0.83$ (mixed)	$g > 0.83$ (liquid)
Instrument (measurement range)			
FSSP (15 to 45 µm)	No	Yes	Yes
Nevzorov probe (LWC > 0.003–0.005 g m^{-3})	No	Yes	Yes
CPI (15 µm to 2.3 mm)	Yes	Yes	No

cal and dynamical conditions. For these reasons, we also included the air mass origin in the classification, which was determined from the analysis of back trajectories computed with the NOAA HYSPLIT model (Hybrid Single-Particle Lagrangian Integrated Trajectory model; Stein et al., 2015). The back trajectories can be classified into two groups: the air masses originating from the north (over sea ice or open water of the Arctic Ocean and Greenland Sea) that are cold and clean, and the air masses more continental which have traveled over more polluted regions in the south and/or east. We made the choice of only two temperature regimes and two main air mass origin in order to ensure representative and statistically significant datasets for each class. Table 5 shows that all the cold situations are correlated with a north origin air mass (blue in Table 5). Among the 12 warm situations, 7 correspond to air masses originating from the north (green in Table 5) and 5 from the south/east (red in Table 5). So, at the end, this classification leads to only three types of situations: (i) cold cloud top temperature situations with air masses originating always from the north (hereafter referred to as COLD cases); warmer situations with air masses which originate either (ii) in the north (hereafter WARM_NO cases) or (iii) from the continent: south and east (hereafter WARM_SO cases).

The mean vertical profiles of temperature of these three regimes are displayed in Fig. 3. The results show a well-pronounced temperature inversion ($\sim -10\,^{\circ}$C) for the WARM_SO situations, whereas WARM_NO cases do not exhibit such clear temperature inversion. The COLD situations are characterized by a temperature of $-20\,^{\circ}$C at cloud top and by weather situations dominated by cold air outbreaks from higher latitudes (Gayet et al., 2009).

3 Vertical properties of liquid droplets and ice crystal particles within MPCs

The purpose of this section is to provide a quantitative assessment of the average microphysical and optical proper-

Table 5. Classification of the MPC situations according to temperature regimes and air mass origins.

Experiment	Date	Mean T_{Top} (°C)	Air mass origin N: north (Arctic Ocean) S/E: south or east (continental)	Regime
ASTAR 2004	15 May	−16.5	N	COLD
	22 May	−8.5	S	WARM_SO
	25 May	−8	N	WARM_NO
	5 June	−11	N	WARM_NO
ASTAR 2007	2 April	−21	N	COLD
	3 April	−16	N	COLD
	7 April	−22	N	COLD
	8 April	−19	N	COLD
	9 April	−21	N	COLD
POLARCAT 2008	31 March	−15	N	WARM_NO
	1 April	−10	N	WARM_NO
	10 April	−14	N	WARM_NO
	11 April	−14	N	WARM_NO
SORPIC 2010	4 May	−13	S/E	WARM_SO
	5 May	−11	S/E	WARM_SO
	6 May	−13	S/E	WARM_SO
	9 May	−15	S	WARM_SO
	10 May	−13.5	N	WARM_NO

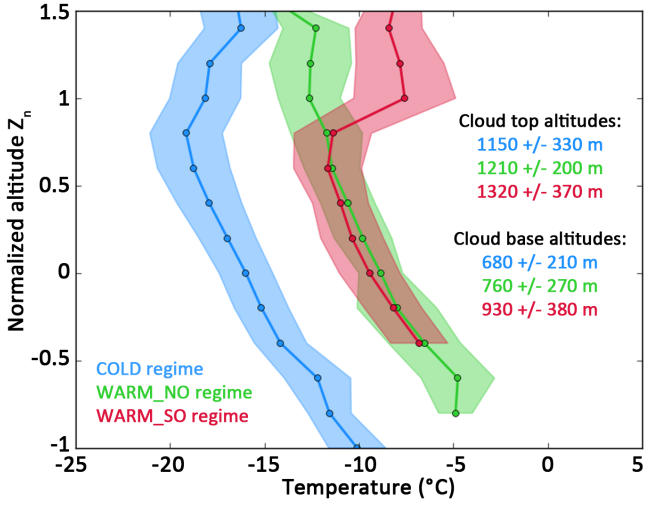

Figure 3. Vertical profiles (normalized altitude) of the mean temperature for each regime. Shaded spreads represent the standard deviation. The mean cloud base and top altitudes and their standard deviation for each regime are indicated.

ties of the MPC cloud layers at a spatial scale of approximately 100 m. The vertical profiles presented in this study come from aircraft in situ measurements and are obtained from several distinctive clouds. It should be emphasized that these profiles cannot be strictly regarded as vertical and instantaneous profiles (each ascending or descending flight sequence is generally made in 5 to 10 min). It differs from the remote sensing measurements that usually provide snapshots of the same cloud.

3.1 Liquid phase properties

Figure 4 displays the average vertical profiles expressed with the normalized altitude reference for the liquid phase properties: the extinction coefficient, the droplet number concentration, the liquid water content and the effective diameter (Fig. 4a to d). These profiles are obtained using FSSP-100 or Nevzorov probe measurements and constrained by PN g values greater than 0.8. In this figure, the average profiles for liquid properties are discriminated for each environmental conditions class: COLD in blue, WARM_NO in green and WARM_SO in red. The mean profile corresponding to the average over all situations (or campaigns) is also shown (in black). The average vertical distribution for the liquid droplet number size distribution is shown in Fig. 4e.

The MPC properties are characterized by increasing values of LWC with altitude. LWC mean values range between 0.1 g m^{-3} at the bottom of the liquid layer and nearly 0.2 g m^{-3} close to the cloud top. The concentration of cloud droplets remains nearly constant throughout the MPC layers with mean values around 120 cm^{-3}. However, smaller values are observed near the cloud top. Clouds corresponding to the WARM_SO situations are characterized by larger values of droplet concentration and LWC (200 cm^{-3} and 0.3 g m^{-3}) compared to the COLD and WARM_NO cases. This is related to the fact that air masses originating from midlatitudes are more humid. The extinction coefficient profiles are

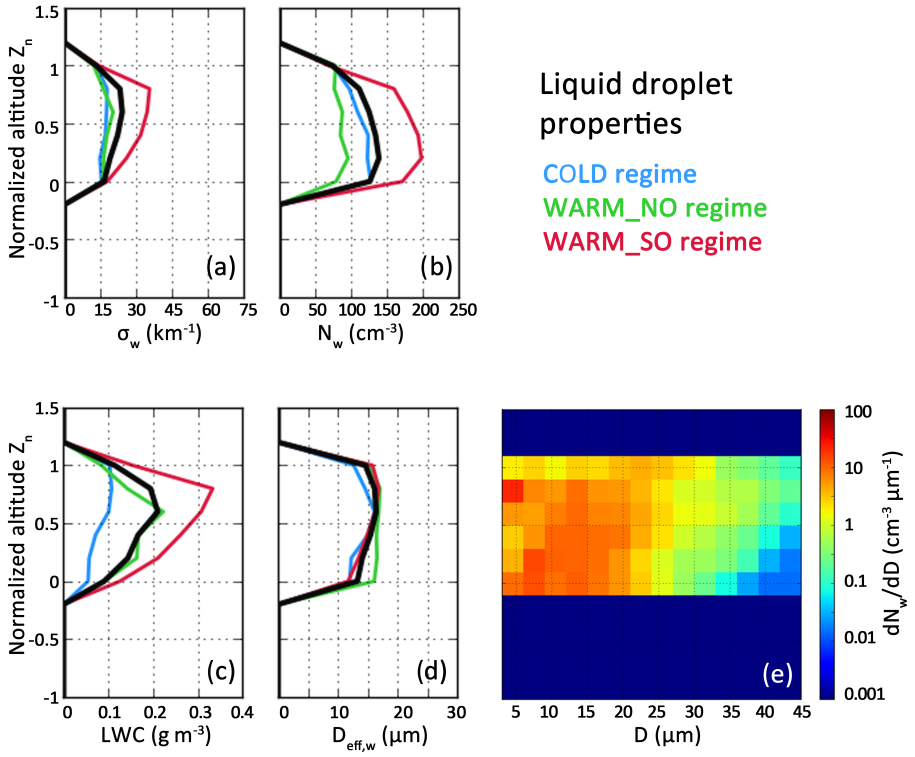

Figure 4. Vertical profiles (expressed in normalized altitude) of liquid droplet properties from FSSP or Nevzorov probe measurements (3–45 µm size range): **(a)** extinction coefficient, **(b)** droplet concentration, **(c)** LWC, **(d)** effective diameter for the three regimes and averaged over all the campaigns and **(e)** averaged droplet size distribution for all the campaigns.

correlated with the LWC measurements, indicating that liquid droplets mainly drive the optical properties of the upper MPC layers. This is consistent with the observed shape of the scattering phase function at cloud top displayed in Fig. 2. The extinction coefficient presents maximum values in the upper part of the cloud (average around 25 km^{-1}) and smaller extinction in the lower part of the liquid layer (down to 15 km^{-1}). Finally, the vertical profiles of the effective diameter (Fig. 4a) and droplet number size distribution (Fig. 4e) are consistent with the extinction coefficient, LWC and droplet concentration. Indeed, the effective diameter is proportional to the ratio of the LWC to the extinction coefficient. The cloud layers dominated by the liquid phase exhibit small droplet sizes, with a slight increase of the diameter from cloud base to cloud top (from 10 to 15 µm).

The main features of the vertical distribution for the liquid phase properties are in agreement with previous observations (e.g., Lawson et al., 2001; McFarquhar et al., 2007 or Jackson et al., 2012). These studies focused on MPCs in the western Arctic region under meteorological situations that can be connected to the ones presented in our work. Lawson et al. (2001) studied a boundary layer MPC in spring over the Beaufort Sea during the First International Satellite Cloud Climatology Regional Experiment Arctic Cloud Experiment (FIRE-ACE). The temperature range lied between −22 and −25 °C. This case could be regarded as the COLD situations in our study. Lawson et al. (2001) showed LWC values around 0.15 g m^{-3} and droplet concentration close to 200 cm^{-3}.

McFarquhar et al. (2007) merged four MPC situations (corresponding to 53 cloud profiles) in autumn over Barrow and Oliktok Point, Alaska, during the Mixed-Phase Arctic Cloud Experiment (M-PACE). The MPCs were associated with a low-level northeasterly flow over the ice pack resulting in persistent roll clouds at low-level altitude. Cloud top temperatures lied between −12 and −16 °C. These situations can be related to our COLD and WARM_NO cases. They also observed the increase of liquid droplet size, LWC and number concentration with the altitude. The LWC range (0.15–0.19 g m^{-3}) is consistent with our study but the droplet size range (from 14 µm at cloud base to 22 µm at cloud top) is slightly larger and the droplet number concentrations significantly lower (between 23 and 72 cm^{-3}). Finally, Jackson et al. (2012) merged 41 MPC profiles during the Indirect and Semi-Direct Aerosol Campaign (ISDAC). They observed liquid droplet properties with mean LWC around 0.15 g m^{-3} at cloud top, droplet size from 8 to 16 µm and droplet concentration around 150 cm^{-3}. These results are consistent with our observations of the liquid phase within MPCs observed over the Greenland and Norwegian seas.

3.2 Ice phase properties

The ice crystal properties derived from the CPI measurements when the PN g values are lower than 0.83 are displayed in Fig. 5 with the same representation as the one used for the liquid phase. In the following, the ice crystal concentration corresponds to particles larger than 100 µm in order to minimize the effect of potential shattering artifacts on this parameter (see Febvre et al., 2012). However, the extinction coefficient, the ice water content, the effective diameter and particle size distribution are determined using all CPI images excluding those identified as liquid droplets. This choice has been made to be consistent with previous studies and allow for accurate comparisons with microphysical parameters obtained during western Arctic campaigns. Averaged values of ice crystal concentration (N_i) and extinction coefficient (σ_i) are around $3\,L^{-1}$ and $0.4\,km^{-1}$, respectively. IWC and effective diameter ($D_{eff,i}$) display mean values ranging from 0.01 to $0.035\,g\,m^{-3}$ and from 80 to 130 µm, respectively. No clear trend in the mean profiles of these properties is observed, as no significant correlation with height is found. However, the values of these parameters decrease to nearly zero at cloud top ($Z_n = 1$). This indicates that the cloud top layer is almost exclusively composed of supercooled liquid droplets and eventually a very low concentration of small ice crystals as shown by the PSD in Fig. 5e. These results corroborate the findings from the previous experiments such as the ISDAC and M-PACE campaigns in the western Arctic (McFarquhar et al., 2011; Jackson et al., 2012). These studies were based on 53 cloud profiles during the M-PACE campaign (McFarquhar et al., 2011) and 41 cloud profiles during the ISDAC campaign (Jackson et al., 2012). The ice crystal properties of single-layer MPCs observed over the Beaufort Sea region did not show any significant vertical variability.

Typical IWC and particle concentration (for crystals with size larger than 125 µm) values lied between 0.006 and $0.025\,g\,m^{-3}$ and between 1.6 and $5.6\,L^{-1}$ for the M-PACE situations. These values are similar to those of the COLD and WARM_NO cases of the present study. Averaged values of IWC and particle concentration during ISDAC are in the range of the WARM_SO situations of the present work with values around $0.02\,g\,m^{-3}$ and $0.27\,L^{-1}$, respectively, for the ISDAC situations. The average ice crystal size observed during M-PACE is around 50 µm, which is smaller than the typical size found in our study. It could be explained by less efficient WBF and riming processes and smaller droplet number also observed during M-PACE.

Deeper in the precipitation layer, closer to the sea level ($Z_n < -0.5$), no general trend can be depicted as ice crystal properties show a large variability. Yet, no ice crystals were found in this region for the WARM_SO situations, whereas the ice precipitation reached the surface ($Z_n = -1$) for the COLD and WARM_NO regimes.

The particle shape vertical distribution was also investigated based on the CPI images. It can provide insight on the main microphysical growth processes occurring in such MPCs. Figure 6 displays the particle shape distributions relative to number and mass concentration with Z_n (Fig. 6a and b) and temperature (Fig. 6c and d). For this purpose, particle shapes have been automatically classified by the algorithm developed at LaMP (see details in Lefèvre, 2007). In addition, the resulting classification was supported by an accurate human-eye visualization in order to control the results and avoid the main shortcomings linked to the automatic classification. As indicated above, only particles with size greater than 100 µm were taken into account in order to avoid misclassification of smaller particles and shattering artifacts.

Our results clearly show that rimed and irregular ice crystals are dominant within MPCs (up to 80 % of the total). In particular, irregular ice particles are encountered at all altitudes and temperatures. They account for 30 to 50 % of the total number concentration (and between 20 and 30 % of mass concentration) depending on the altitude or temperature of the MPC layer. Rimed particles are predominant inside the liquid-containing cloud layer ($0 < Z_n < 1$) with a contribution up to 40 % in number (60 % in mass) where low temperatures (below −18 °C) are observed.

An interesting feature is the significant occurrence (around 40 %) of ice crystals with a predominant a axis growth at all cloud levels. Indeed, plates, side planes and stellars are the dominant habits among the regular shapes regardless of the cloud layer altitude.

Below the cloud ($Z_n < 0$), precipitating ice crystals are characterized by a mass concentration dominated by rimed particles and a large number concentration fraction of irregular ice crystals.

Overall, these results agree with the ones presented in McFarquhar et al. (2007) based on in situ observations of MPCs during the M-PACE experiment. McFarquhar et al. (2007) also stated that small supercooled water droplets dominated the upper layer of the cloud while larger ice particles were present in the lower part and below the cloud (including irregular, aggregate or rimed-branched crystals). But our results differ since they observed a fraction of needles and columns particles a lot larger than in our study (respectively, up to 50 % below the cloud versus less than 10 %). On the contrary, our results are not in agreement with the observations described in Korolev et al. (1999); this is because they observed even less regular ice crystals: irregular-shaped ice crystals accounted for up to 98 % of the total number of ice particles. This disagreement could be explained by two reasons. First, Korolev et al. (1999) considered a wide variety of clouds sampled in the Canadian and US Arctic (stratocumulus and cirrus at temperatures ranging from 0 to −45 °C and up to 7.5 km altitude), whereas the present study focuses only on MPCs in the Svalbard region at low altitudes. The disagreement may also stem from the different image processing used in these studies. For instance, Korolev et al. (1999) took into account particles larger than 40 µm (while a 100 µm threshold was used in our study) and two ice crystal shapes:

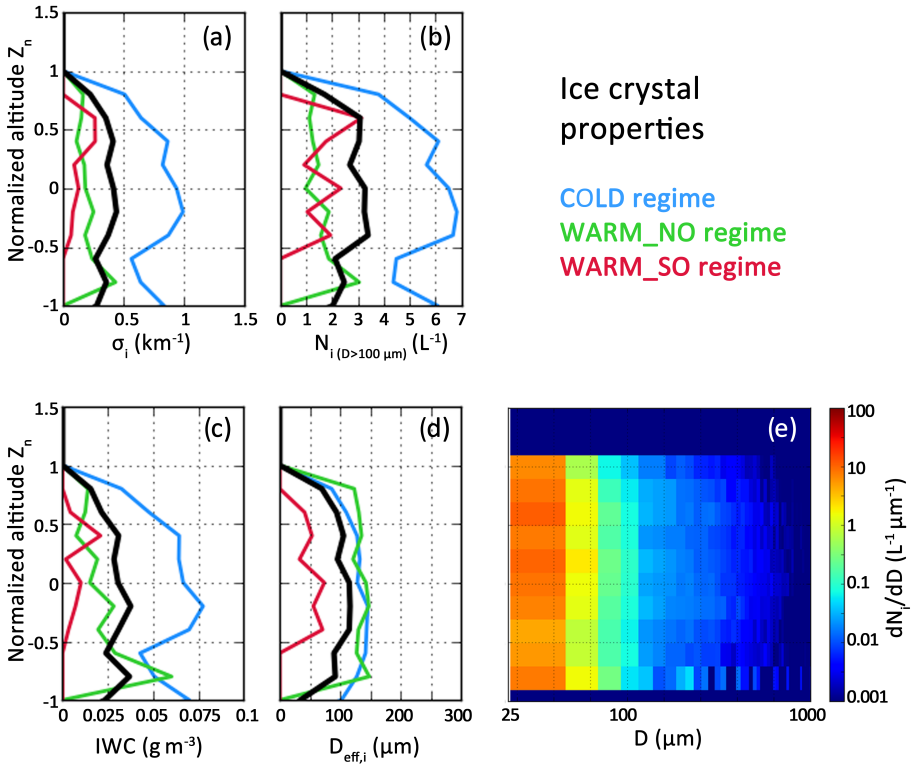

Figure 5. Vertical profiles (expressed in normalized altitudes) of ice crystal properties from CPI measurements (15 µm–2.3 mm size range): **(a)** extinction coefficient, **(b)** ice crystal concentration, **(c)** IWC, **(d)** effective diameter for the three regimes and averaged over all the campaigns and **(e)** averaged particle size distribution for all the campaigns.

pristine (defined as faceted single ice particles) and irregulars were considered (while 10 particle shapes were accounted for in our results).

3.3 Discussion on statistical vertical profiles

The quantitative estimates of the separate properties of droplets and ice crystals may provide insight on the microphysical processes occurring in MPCs. These processes are involved in the MPC life cycle, in particular to maintain the coexistence of liquid droplets and ice crystals, leading to its persistence (Morrison et al., 2012). More specifically, the increase with height of droplet size and LWC observed in the vertical profiles is consistent with a condensational growth process. The slight decrease of LWC and number concentration observed at the very top of the cloud may be due to turbulent mixing (Korolev et al., 2015) and entrainment of dry air. Additionally, the data collected in this part of the cloud may also lead to a slight underestimation of the LWC since a mixing of cloudy and cloud-free patches could be averaged together given the sampling resolution (i.e., 100 m). The analysis of the vertical profiles of ice properties and ice crystal shapes (see Fig. 6) shows that the presence of pristine particles, mainly plates and stellars, could be linked to a very fast ice crystal growth by vapor deposition due to the WBF process in which ice crystals grow at the expense of liquid droplets. The large contribution of rimed particles confirmed that riming process shall be significant in a mixed-phase cloud. The prevalence of irregular particles is in agreement with the previous studies from Korolev et al. (1999) and McFarquhar et al. (2007) and suggests that aggregation growth processes or a combination of several growth mechanisms are involved. This also indicates that turbulence or mixing into the cloud may have an important influence by redistributing the precipitating ice crystals in the upper cloud levels. Measurements of the vertical wind speed (which are not available for these campaigns) would be helpful to confirm this hypothesis.

Theoretical adiabatic LWC has also been determined assuming a non-entraining parcel of moist air rising and reaching saturation. It is calculated from the pressure and temperature measurements from cloud base to cloud top. These theoretical values are then compared to the observed LWC values to evaluate the influence of turbulence or mixing effects on LWC as well as the efficiency of ice growth by WBF process or riming processes. The profiles of the adiabatic ratio (the ratio of the adiabatic LWC to the observed LWC) are displayed in Fig. 7. Subadiabatic values are found for all meteorological regimes. This means that processes responsible for a decrease of LWC compared to the adiabatic prediction

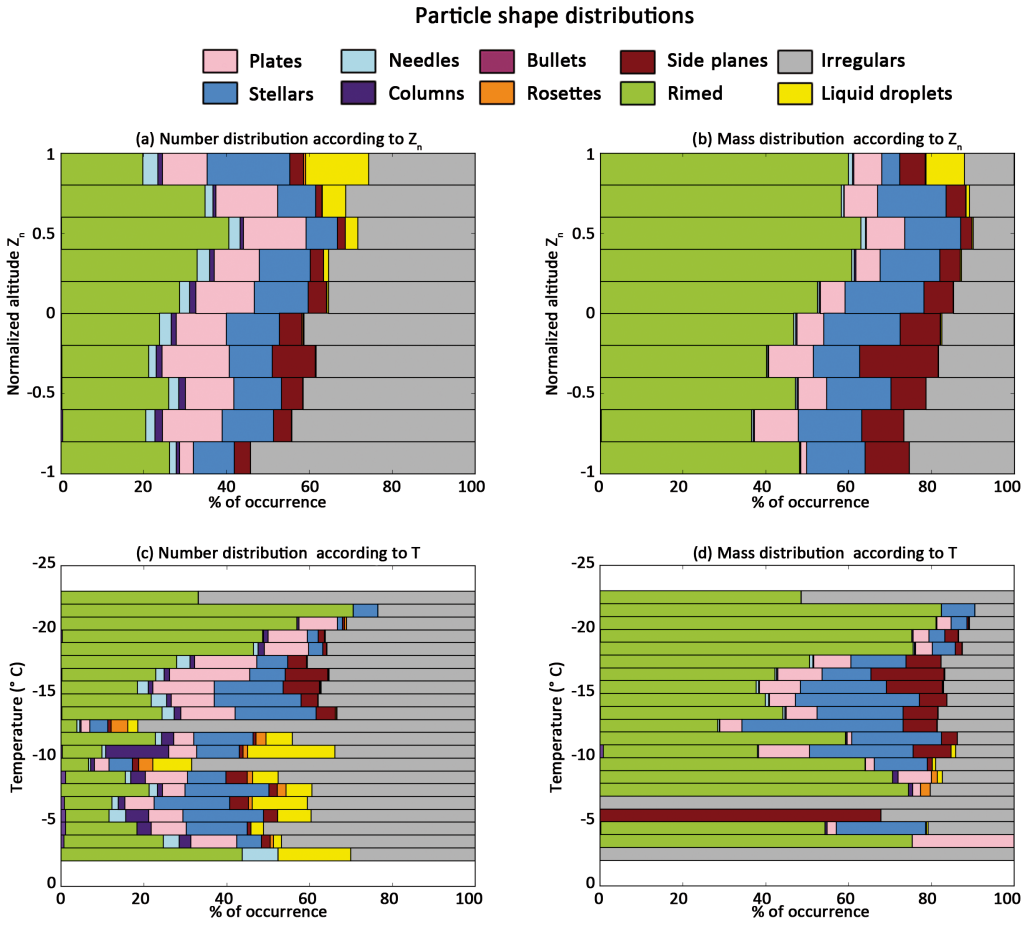

Figure 6. Vertical profiles of particle shapes (from CPI measurements and for particles larger than 100 µm) according to normalized altitude **(a, b)** and temperature **(c, d)**. Distributions are displayed according to particle number **(a, c)** and mass **(b, d)**.

are prevalent. In particular, this strengthens the assumption that a turbulent entrainment of dry air, resulting in the evaporation of liquid droplets, may occur at cloud top. Moreover, this confirms that the WBF and riming processes are efficient and responsible for the decrease of LWC compared to adiabatic values. These statements are in agreement with the study from Jackson et al. (2012), who showed for several boundary layer MPCs over Barrow, Alaska, during the ISDAC campaign that the subadiabatic profile of LWC and the decreasing droplet concentration at cloud top may be associated with the ice crystal growth processes involving the liquid phase (riming and WBF) and/or the entrainment of dry air from above.

However, Figs. 4 and 5 also showed significant differences in cloud vertical profiles from one regime to another. The COLD situations exhibit the largest values for ice properties (IWC up to $0.075\,\mathrm{g\,m^{-3}}$, N_i up to $8\,\mathrm{L^{-1}}$) together with the lowest LWC values ($<0.1\,\mathrm{g\,m^{-3}}$). On the contrary, the WARM_SO profiles are characterized by the largest liquid droplet concentrations, extinction coefficient and LWC values ($\sim 200\,\mathrm{cm^{-3}}$, $40\,\mathrm{km^{-1}}$ and $0.3\,\mathrm{g\,m^{-3}}$, respectively) and low values of IWC, extinction and size of ice crystals ($\mathrm{IWC} < 0.01\,\mathrm{g\,m^{-3}}$, $\sigma_i < 0.2\,\mathrm{km^{-1}}$ and $D_{\mathrm{eff}} < 50\,\mu\mathrm{m}$, respectively). Thus, in the WARM_SO regime, it seems that the number of ice crystals is too low and their size too small to efficiently consume liquid droplets by WBF or riming processes (Pruppacher and Klett, 1978), explaining on one hand the prevalence of the liquid phase and on the other hand that the precipitating ice crystals below the cloud do not reach the surface. Moreover, the habit classification as a function of the temperature shows differences between the COLD regime and the WARM regimes (not shown here). This concerns, in particular, the presence of some large droplets in the WARM regimes which are not present in the COLD regime and the presence of plate and stellar particles below $-10\,^{\circ}\mathrm{C}$ or around $-4\,^{\circ}\mathrm{C}$, which is consistent with the classical ice crystal morphology diagram (Libbrecht, 2005; Nakaya, 1954).

The adiabatic ratio, shown in Fig. 7, confirms this assumption where larger values are encountered for the WARM_SO situations. Indeed, a large adiabatic ratio denotes that processes responsible for the depletion of liquid droplets (mainly riming or WBF) are relatively less efficient.

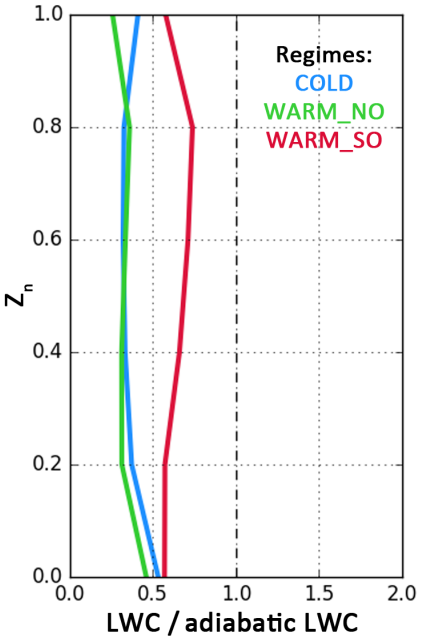

Figure 7. Vertical profiles of the ratio of measured LWC over theoretical adiabatic LWC for the three regimes.

The ice crystal properties relative to the WARM_NO situations are similar to the WARM_SO cases, except for the effective diameter where values are similar to the COLD regime ($D_{\mathrm{eff,i}} > 100\,\mu\mathrm{m}$). The liquid droplets for this regime exhibit the lowest concentrations ($< 100\,\mathrm{cm}^{-3}$) and an intermediate LWC value (around $0.2\,\mathrm{g\,m}^{-3}$).

The meteorological classification used in our study is also based on the air mass origin since it shall impact the cloud microphysical properties, as shown in Gultepe and Isaac (2002). In particular, COLD and WARM_NO situations characterized by a northern air mass origin should be associated with more pristine conditions and drier air compared to the WARM_SO situations. Airborne in situ aerosol measurements were only available during the POLARCAT 2008 campaign (with particle counters). However, nearly continuous aerosol measurements (with particle counters and sizers) but ground based were performed at the Mount Zeppelin station (Ny-Ålesund, Svalbard, 475 m above sea level, 79° N, 12° E) during a period encompassing the ASTAR and SORPIC campaigns. Even though these measurements do not provide an accurate estimate of the aerosol concentration at the exact location and time when the clouds were sampled, they still give an indication of the background aerosol loading. Based on these measurements, the mean aerosol number concentrations were 230, 120 and $330\,\mathrm{cm}^{-3}$ for the COLD, WARM_NO and WARM_SO, respectively; we can conclude that pristine conditions are encountered for air masses originating from the north and that cloud measurements performed under WARM_SO conditions are more likely to be affected by long-range transport of pollution for the south/east.

The prevalence of the ice phase for the COLD regime is thus consistent both with the cold temperature and the pristine conditions associated with northern air masses. Despite similar air mass origins, the WARM_NO cases exhibit a smaller concentration of ice crystals than the COLD situations. This suggests that the influence of the cloud top temperature prevails to promote the growth or production of ice crystals. The WARM_SO cases which combine warm temperatures and continental air masses clearly show that the ice crystal growth or production is reduced, as well as the precipitation efficiency, and that the liquid phase dominates the cloud structure.

Additionally, the comparison of the vertical profiles of MPC properties of the present work to the previous studies concerning the western Arctic in Sect. 3.2 showed that the cloud properties for the COLD and WARM_NO situations agree with that of M-PACE (REF), in particular in terms of ice concentration and IWC. The WARM_SO cases agree more with the ISDAC situations, in particular the low ice concentration. Jackson et al. (2012) explained the very low ice concentration observed during ISDAC as a consequence of more polluted situations encountered (compared to M-PACE) that might reduce the secondary ice crystal production efficiency (thermodynamic indirect effect). This conclusion is thus in accordance with our assumption that the air mass coming from the south may be more impacted by pollution and may reduce the ice growth efficiency.

These analyses show that microphysical properties of Arctic MPCs over the Greenland and Norwegian seas are closely linked to the cloud top temperature regime and the environmental conditions such as the air mass origin. Similar conclusions have already been made for MPCs in the western Arctic regions by Gultepe and Isaac (2002) who demonstrated the impact of the air mass origin (Pacific Ocean or Arctic Ocean) on the MPC microphysical properties.

However, a more thorough analysis involving collocated in situ aerosol measurements is obviously needed to confirm these findings. For instance, our results are somehow consistent with Lance et al. (2011) or Rangno and Hobbs (2001) who showed that "polluted" MPCs exhibit higher droplet concentrations and smaller ice-precipitating particles compared to "clean" MPCs. A large number of droplets are expected to reduce the riming process and thus contribute to the large observed values of LWC (as liquid droplets are not consumed by the ice crystals).

To go further into the analysis of our microphysical dataset, additional measurements of key parameters are necessary. In particular, quantifying the mechanisms responsible for the formation and growth of droplets and ice crystals within MPCs by measuring the numbers of IN and cloud condensation nuclei (CCN) is needed. It would enable us to perform an accurate ice closure and to quantify, for example, the possible impact of secondary ice production processes).

A better characterization of the dynamical processes at cloud scale, with accurate high spatial resolution measurements of vertical wind velocities into and around the MPCs would also be necessary. For instance, upward air motion and turbulent entrainment of air from above the cloud are critical to maintain liquid water in MPCs. Accurate humidity measurements would also be needed to better identify condensational growth of ice crystals (WBF process or direct condensation of water vapor on ice, as described by Korolev, 2007) and resolve the issue of turbulence and mixing at cloud edges and into clouds. All these parameters, along with radiative flux measurements, are of primary importance to constrain our assumptions on the microphysical processes.

At last, coupling our results (and further observations with new parameters and improved instrumentation) with modeling is of course the best way to quantify the relative impact of each process on the MPC lifetime. However, such work remains beyond the scope of the present study.

4 Parameterizations of key microphysical parameters

In Sect. 3, we have shown that in situ data provide a detailed characterization of the microphysical and optical properties of MPCs. These measurements can also be used to develop cloud parameterizations and to evaluate remote sensing retrieval products or modeling outputs. This section focuses on the key properties and hence parameters which must be better quantified (Morrison and Pinto, 2006), namely (i) IWC (and LWC) – extinction coefficient relationships, (ii) the variability of the ice and liquid water paths, (iii) the temperature-dependent ice crystal concentration and (iv) the liquid water fraction (ratio of LWC over total water content) as a function of the cloud level or temperature.

4.1 Ice and liquid water contents and integrated paths

Linking cloud microphysical and optical properties is an important step in order to model the cloud radiative properties or to constrain/develop remote sensing retrieval methods. In particular, accurate IWC–extinction relationships and integrated properties such as ice and liquid water paths are needed to improve the remote sensing retrieval products and cloud modeling (Heymsfield et al., 2005; Waliser et al., 2009). In this section, we provide such relationships and parameters based on in situ measurements.

Figure 8a and b display the IWC and the LWC measurements as a function of the ice and droplet extinction coefficients, respectively, with the temperature superimposed in color. The averaged values of IWC and LWC over intervals of 0.1 and 2 km^{-1} for the ice and liquid extinction coefficients, respectively, are represented by the grey squares in order to determine the fitting curves (represented by the red lines with the mean absolute error in dashed lines; see Eqs. 3 and 4 below). Ice crystal and liquid droplet extinction coefficients are well correlated with their water content counterparts. The correlation coefficients are high (0.88 for ice and 0.89 for liquid) and the IWC–σ and LWC–σ relationships are nearly linear.

It should also be noted that including the temperature as an additional parameter for the linear fitting did not improve the accuracy of the parameterizations, contrary to previous studies of Heymsfield et al. (2005), Hogan et al. (2006), or Protat et al. (2007, 2016). However, these previous studies concerned tropical and midlatitude clouds and cover a much broader range of temperatures (from −65 to 0 °C, compared to narrower range from 24 to 0 °C in our study).

$$\mathrm{IWC} = 0.076\,\sigma^{1.06} \tag{3}$$

$$\mathrm{LWC} = 0.0016\,\sigma^{1.31} \tag{4}$$

with IWC and LWC in g m^{-3} and σ in km^{-1}.

Integrated properties such as liquid water path (LWP) and ice water path (IWP) are common modeling outputs which suffer from large discrepancies depending on the model specifications (Waliser et al., 2009). Moreover, only a very limited number of studies were devoted to retrieving these properties from in situ measurements in this region of the Arctic. Since the flight legs selected in our study target ascending and descending sequences into single-layer MPCs, in situ measurements can be used to determine IWP and LWP according to the following equation:

$$\mathrm{IWP\ (or\ LWP)} = \int_{\mathrm{ground}}^{\mathrm{cloud\ top}} \mathrm{IWC\ (or\ LWC)}\,(z)\,\mathrm{d}z. \tag{5}$$

We recall that these integrated properties should be considered quasi-instantaneous, as ascending and descending flight sequences are obviously not fully vertical and need about 5–10 min to be performed (compared to the snapshots performed by remote sensing measurements).

Figure 8c displays the ice (green) and liquid (blue) water paths as a function of the cloud top temperature (1 °C intervals). For cloud top temperatures below −20 °C, IWP and LWP reach values close to 30 and 50 g m^{-2}, respectively. The IWP decreases dramatically when the cloud top temperature increases; very low values close to 0 are encountered at temperatures above −8 °C. LWP reaches a maximum of 100 g m^{-2} at −13 °C and the smallest values (around 15 g m^{-2}) are encountered when the cloud top temperature is typically around −18 °C. These findings are consistent with the main previous studies devoted to Arctic MPCs (Hobbs et al., 2001; Pinto, 1998; Pinto and Curry, 2001; Shupe et al., 2006). They reported mean LWP values in the range of 20–70 g m^{-2}, with some maxima up to around 130 g m^{-2}, and IWP mean values less than 40 g m^{-2}. However, one shall note that all these previous studies concerned once again the MPCs in the western Arctic regions (Barrow, Alaska, Beaufort Sea).

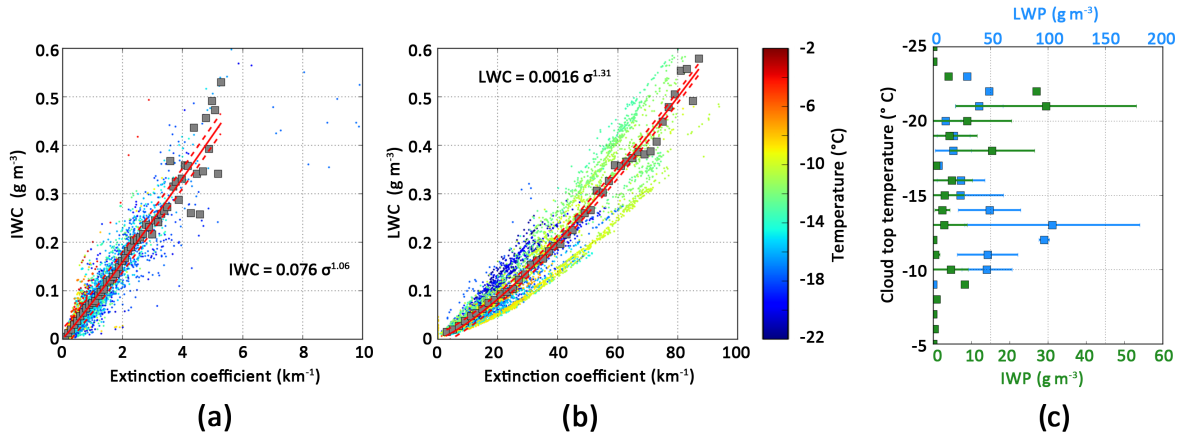

Figure 8. **(a)** IWC and **(b)** LWC as a function of extinction coefficient. Color scale indicates the temperature; grey squares represent the values averaged over extinction coefficient intervals of 0.1 and 2 km^{-1} for IWC and LWC, respectively. The red lines represent the curve fittings and the dashed lines the uncertainties on the fitted relationships (mean absolute errors). **(c)** Ice (green) and liquid (blue) water paths according to the cloud top temperature.

4.2 Ice crystal concentration

The accurate knowledge of the ice crystal concentration is of primary importance to correctly parameterize the initiation and evolution of the ice phase in models and reduce the significant uncertainties in the modeling of the ice/liquid partitioning within MPCs.

Figure 9 shows the maximum number concentration of ice crystals with size greater than 100 µm as a function of the cloud top temperature for each MPC vertical profile. The data points are color-coded according the COLD, WARM_NO and WARM_SO environmental regimes. This figure highlights that the maximum ice concentration varies almost exponentially (figure is in log-lin scale) with the cloud top temperature, with nevertheless a large variability. Thus, a relationship may be fitted in order to parameterize the ice crystal number concentration as a function of temperature in MPCs (Eq. 6, also included in Fig. 9), even though the correlation coefficient is quite low (0.43). The mean absolute error (MAE) is also displayed in Fig. 9 (dotted lines) to estimate the uncertainties on the parameterization.

$$N_{\mathrm{i,max}} = e^{(-0.191 T_{\mathrm{top}} - 1.134)} \text{ with } N_{\mathrm{i,max}} \text{ in } L^{-1} \text{ and } T_{\mathrm{top}} \text{ in } ^{\circ}\mathrm{C} \quad (6)$$

For comparison purposes, the parameterizations of Meyers et al. (1992) and Cooper (1986) for heterogeneous ice nucleation and the parameterization of Young et al. (2017) for primary ice nucleation based on microphysical observations during the Aerosol-Cloud Coupling and Climate Interactions in the Arctic (ACCACIA) campaign are displayed (in purple, orange and brown dashed lines, respectively). The Meyers et al. (1992) parameterization is within the range of the uncertainties of our parameterization. However, it significantly deviates from our relationship for cloud top temperature higher than −15 °C, i.e., for clouds under warm regime. For these regimes, the ice number concentrations can differ by a factor of up to 2 at −10 °C.

The parameterizations of Cooper (1986) and Young et al. (2017) do not match with the present parameterization since the ice crystal concentrations predicted are around 1 order of magnitude lower than the ones in the present study. This difference can be explained by the different seasons, cloud types and locations of the observations used for the parameterization of Cooper (1986) and the fact that the range of their measured concentrations lies within a factor of 10 as they noted.

In contrast, the sampling conditions for the determination of the Young et al. (2017) parameterization are more similar to the present work; they used measurements in Arctic MPCs over the Greenland Sea. The dataset was collected during spring and summer, above open sea, ice sheet and transitions. This variability in the seasons and surface conditions may explain the differences observed compared to the present work. Above all, Young et al. (2017) displayed an averaged concentration, whereas the maximum ice number is presented here. However, even by taking the averaged ice concentrations in the present work, the parameterization does not match with that of Young et al. (2017) (not shown here). Finally, the detailed time series displayed in the Young et al. (2016) and Lloyd et al. (2015) works which present the cases used for the determination of the parameterization of Young et al. (2017) showed that the maximum ice number concentrations frequently displayed values between 1 and 5 L^{-1}, which is in the range of the present parameterization.

Our results could not be compared to more sophisticated parameterizations accounting for supersaturation and aerosol properties (such as (DeMott et al., 2011) since additional data are needed (aerosol and CCN/IN measurements, humidity).

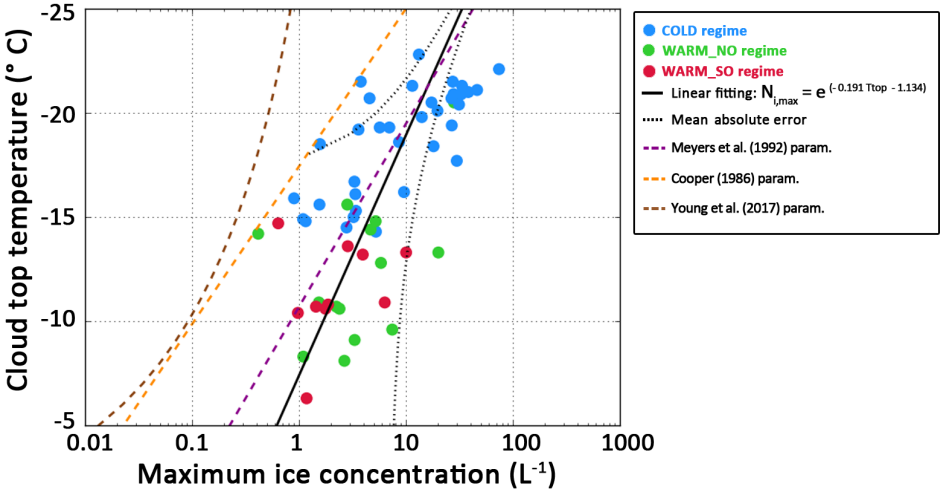

Figure 9. Maximum ice crystal concentration as a function of cloud top temperature. The colored circles represent the values for each profile (with fitting in the black solid line and mean absolute error in dotted lines). The Meyers et al. (1992), Cooper (1986) and Young et al. (2017) parameterizations are also displayed in purple, orange and brown dashed lines, respectively.

These additional data are also necessary to discuss the processes such as the secondary ice production processes which could explain the higher crystal numbers observed in the present study compared to the other works presented in this section.

4.3 Liquid water fraction

The MPC liquid fraction can be determined based on the separate liquid and ice properties presented in Sect. 3. The liquid water fraction (hereafter LWF) is defined as the ratio of LWC over the TWC (IWC plus LWC) at each altitude level.

To our knowledge, very few previous studies have assessed the liquid water fraction in MPCs. Most of them were concerned with MPCs only in western Arctic regions (de Boer et al., 2009; McFarquhar et al., 2007; Shupe et al., 2006).

Figure 10a displays the liquid fraction according to the normalized altitude Z_n. For purpose of comparison, the parameterization from McFarquhar et al. (2007) (hereafter MF07) determined from in situ measurements during M-PACE is also represented in Fig. 10a by the black dotted curve. Our relationship (Eq. 7) significantly deviates from that of MF07.

$$\mathrm{LWF} = 28.4 Z_n + 54.9 \text{ with LWF in \%} \quad (7)$$

They used in situ measurements from 53 profiles in single-layer MPCs sampled over Alaska with temperatures ranging from −3 to −17 °C. As mentioned in Sect. 3, they observed similar ice crystal number concentrations but ice crystals were smaller, with mean effective diameters around 50 µm compared to 100 µm in our study.

Figure 10b shows the liquid fraction according to cloud top temperature. Each point represents the mean value of the liquid fraction determined for each profile. The error bars corresponding to the standard deviation display large values around 80 %, which is indicative of a large variability. Nevertheless, Fig. 10b shows that LWF is well correlated with the cloud top temperature (Eq. 8). The decrease in LWF associated with a decrease of temperature is consistent with Fig. 9 which shows that ice number concentration increases for colder temperatures.

$$\mathrm{LWF} = 2.97 T_{\mathrm{top}} + 121.20 \text{ with LWF in \% and } T_{\mathrm{top}} \text{ in °C} \quad (8)$$

The liquid fraction is also determined at each cloud level as a function of the temperature in Fig. 10c (with 1 °C temperature interval). The same trend as in Fig. 10a is observed. The liquid water fraction increases with decreasing temperature. The relationship between LWF and T is nearly linear with similar slopes for the three regimes (Eq. 9a, b and c for the COLD, WARM_NO and WARM_SO regimes, respectively):

$$\mathrm{LWF} = -3.02\,T + 3.95 \quad (9a)$$
$$\mathrm{LWF} = -3.48\,T + 47.60 \quad (9b)$$
$$\mathrm{LWF} = -1.70\,T + 76.16, \quad (9c)$$

with LWF in % and T in °C.

However, large shifts are observed from one regime to another, especially when comparing the COLD regime to the WARM_NO and the WARM_SO. This shift is clearly linked to the temperature profiles (see Fig. 3). However, one can note that the results for the WARM_NO regime are the ones in the closest agreement with the MF07 parameterization.

In order to compare our results to those of Shupe et al. (2006), we also determined the total liquid water fraction ($\mathrm{LWF_{total}}$) in terms of water paths (LWP/TWP). Figure 10d shows a rather good agreement between the two water path ratios, showing that IWP dominates in the coldest clouds

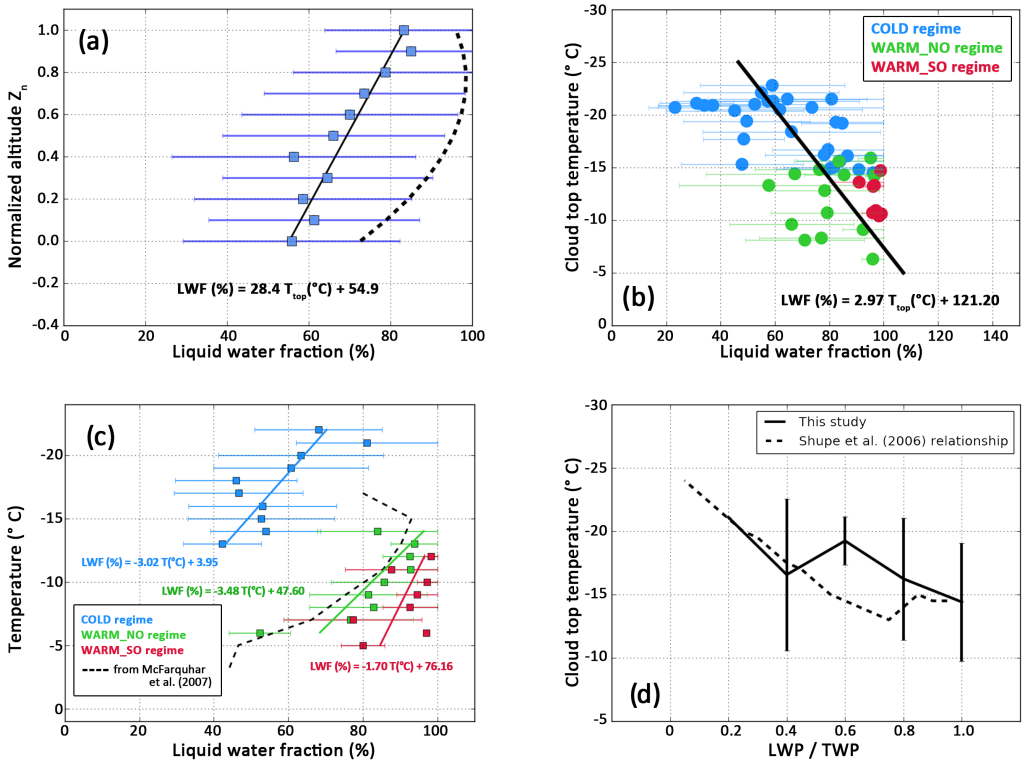

Figure 10. Liquid water fraction according to Z_n **(a)**, cloud top temperature **(b)** and temperature **(c)**. The dotted dashed line in panels **(a)** and **(c)** is the parameterization from McFarquhar et al. (2007) and the solid lines in panels **(a)**, **(b)** and **(c)** are the fittings for the present study. **(d)** Ratio of LWP over total water path (TWP) according to cloud top temperature. The solid line refers to the present study and the dotted line refers to Shupe et al. (2006).

(T_{top} around −20 °C on average). On the contrary, LWF_{total} is more important in the warmer MPCs (T_{top} above −15 °C). However, such liquid fraction determination must be taken with care since it integrates the ice region below the clouds (de Boer et al., 2009).

5 Conclusions and outlook

In this study, a characterization of Arctic boundary-layer mixed-phase clouds microphysical properties has been performed. In situ data from four airborne campaigns over the Greenland Sea and the Svalbard region are compiled and analyzed. The dataset represents in total 18 flights and 71 vertical profiles in MPCs (more than 350 min of cloud in situ observations). Cloud phase discrimination is achieved and vertical profiles of the number, size, mass and shape of ice crystals and liquid droplets within MPCs are determined.

The main conclusions of the present work are summarized as follows:

i. Liquid phase is mainly present in the upper part of the MPCs with high concentration of small droplets ($N_w \sim 120\,cm^{-3}$, $D_{eff,w} \sim 15\,\mu m$) and averaged LWC around $0.2\,g\,m^{-3}$. Ice crystals are present everywhere in the MPCs with no significant vertical variability ($N_i \sim 3\,L^{-1}$, $D_{eff,i} \sim 100\,\mu m$, $IWC \sim 0.025\,g\,m^{-3}$), but mainly in the lower part, and precipitate down to the surface. The morphology study of ice crystal images showed that irregular and rimed particles prevail over stellar and plate habits.

ii. The vertical profiles of the microphysical properties and the shape distribution can also be used to provide insight on the microphysical processes occurring in MPCs. It is likely that adiabatic lifting (condensation) is the main process for liquid droplet initiation and growth, and that evaporation at cloud top due to entrainment of dry air seems to occur. In the cloud layer, where liquid droplets and ice crystals coexist, the Wegener–Bergeron–Findeisen and riming processes are the main mechanisms involved in the ice crystal growth. The large occurrence of irregular particles highlights the fact that the ice crystals undergo a variety of growth processes, and the turbulence in the MPC life cycle is efficient for mixing the cloud.

iii. The analysis of the scattering phase function showed a very high correlation between optical properties and liquid to ice fraction within the MPC layers.

iv. Statistical analysis exhibits significant differences in the vertical profiles of MPC properties depending if the cloud top is cold or warm and if the air mass originates from higher or lower latitudes. The largest droplet concentration and LWC values observed ($200\,cm^{-3}$, $0.3\,g\,m^{-3}$, respectively) are associated with the warm temperature regime, with air mass originating from the south/east (continental areas). For these situations, at the same time, very low values of ice crystal size and IWC are observed (IWC $< 0.01\,g\,m^{-3}$, $D_{eff,i} \sim 50\,\mu m$). On the contrary, the colder situations exhibit large values of ice contents especially when air masses originate from the north (IWC $\sim 0.075\,g\,m^{-3}$). These results underline the importance of the air mass origin and the cloud top temperature as well as the need for simultaneous aerosol measurements (sources, transport, physical and chemical properties) in connection with the MPC properties to study the cloud–aerosol interactions and improve the understanding of ice and liquid formation processes.

v. The main results of the present work were compared to the previous studies which concern mainly MPCs in the western Arctic region. The main findings showed that the properties of the COLD and WARM_NO situations (large values of ice properties) of the present work are consistent with the rather clean situations of previous western Arctic studies such as M-PACE. On the contrary, the MPC properties of the WARM_SO cases (prevalence of liquid phase and very low values of ice properties) are more in agreement with the more polluted situations in the western Arctic, such as ISDAC. These findings confirm that the MPC properties are strongly linked to the environmental conditions such as temperature and air mass origin.

vi. Several parameterizations for remote sensing or modeling are proposed. This concerns the determination of IWC (and LWC) – extinction relationships, ice and liquid integrated water paths, the ice concentration and liquid water fraction. Comparisons with the few previous works available in the literature showed, in general, a good agreement. Obviously, the application range of the established relationships is only for Arctic MPCs and temperature range between 0 and $-23\,°C$. A next step to the present work will be to apply the proposed parameterizations to remote sensing algorithms and modeling to investigate their relevance.

This study provided, for the first time, a statistical analysis of Arctic MPC in situ data from four airborne campaigns located in the eastern Arctic region. An accurate characterization of the vertical variability of liquid droplet and ice crystal properties has been made, allowing the development of parameterizations.

Further studies should involve new measurement techniques to provide accurate characterization of cloud phase and microphysical properties, in particular for the small particles. This will allow to complete and validate the present results. For example, instruments like the small ice detector (SID-3; Ulanowski et al., 2014; Vochezer et al., 2016) or the cloud particle spectrometer with polarization detection (CPSPD; Baumgardner et al., 2014) should provide valuable measurements to differentiate droplets from ice crystals even at sizes lower than 50 µm. Both probes are an open path to avoid shattering artifacts. Additionally, accurate measurements of humidity and aerosol (CCN and IN) remain an important shortage in order to deepen the analysis of microphysical processes and to realize ice and liquid closure and better understand the life cycle and persistence of such particular clouds. For this purpose, a modeling study of cloud microphysics shall be of help. Finally, by characterizing clouds at very low altitude levels, this work can be useful in future studies for validation/evaluation of space remote sensing observations and retrieval products (A-Train, EarthCare, etc.), since these measurements are known to have important shortcomings near the surface.

Data availability. All the information to access to the cloud in situ data is on the Arctic data portal website: http://climserv.ipsl.polytechnique.fr/arcticportal/.

Appendix A: Data processing of in situ measurements

The methodology developed by Lawson and Baker (2006) to derive the IWC from 2-D particle images recorded by the CPI instruments is applied (Eq. A1 below).

$$\mathrm{IWC} = \frac{0.135 \sum_{\mathrm{i}} X_{\mathrm{i}}^{0.793}}{V}, \quad \text{(A1)}$$

where V is the sample volume and X_{i} is the mass parameter for each crystal image defined by Lawson and Baker (2006) as follows:

$$X_{\mathrm{i}} = \frac{A_{\mathrm{i}} \times W_{\mathrm{i}} \times 2 \times (L_{\mathrm{i}} + W_{\mathrm{i}})}{P_{\mathrm{i}}}. \quad \text{(A2)}$$

A_{i}, W_{i}, L_{i} and P_{i} are the area, width, length and perimeter of the crystal image i, respectively.

The extinction coefficient (σ) and the effective diameter (D_{eff}) are determined from CPI and FSSP measurements as follows:

$$\sigma_{\mathrm{ice\ (or\ liquid)}} = 2 \times \frac{\sum_{i} A_i}{V} \quad \text{(A3)}$$

$$D_{\mathrm{eff,ice\ (or\ liquid)}} = C \times \frac{\mathrm{IWC\,(or\ LWC)}}{\sigma_{\mathrm{ice}}\ (\mathrm{or}\ \sigma_{\mathrm{liquid}})}, \quad \text{(A4)}$$

with constant $C = 3000\,\mathrm{mm^3\,g^{-1}}$ according to Gayet et al. (2002).

The LWC derived from the Nevzorov probe measurements is calculated according to Korolev et al. (1998):

$$\mathrm{LWC_{Nevzorov}} = \frac{P_{\mathrm{LWC}} - \left(\frac{P_{\mathrm{TWC}} \times \varepsilon_{\mathrm{LWC,i}} \times S_{\mathrm{LWC}}}{\varepsilon_{\mathrm{TWC,i}} \times S_{\mathrm{TWC}}}\right)}{L_{\mathrm{v}} \times S_{\mathrm{LWC}} \times U \times \left(\varepsilon_{\mathrm{LWC,l}} - \frac{\varepsilon_{\mathrm{LWC,i}} \times \varepsilon_{\mathrm{TWC,l}}}{\varepsilon_{\mathrm{TWC,i}}}\right)}, \quad \text{(A5)}$$

where P_{LWC} and P_{TWC} are the power supplied to the LWC and TWC sensors to maintain the constant temperature of the wire.

S_{LWC} and S_{TWC} are the surfaces of the sensors, L_{v} is the latent heat of vaporization and U is the true airspeed.

The epsilon terms refer to the collection efficiencies of liquid droplets (l index) or ice crystals (i index) on the LWC and TWC sensors. These efficiencies are set as follows:

- $\varepsilon_{\mathrm{LWC,l}} = 0.76$; see Schwarzenboeck et al. (2009);
- $\varepsilon_{\mathrm{LWC,i}} = 0.11$, following Korolev et al. (1998);
- $\varepsilon_{\mathrm{TWC,l}} = 1$, according to Korolev et al. (1998) for droplets with size around 25 µm; and
- $\varepsilon_{\mathrm{TWC,i}} = 1$, following Schwarzenboeck et al. (2009). It should be noticed that taking $\varepsilon_{\mathrm{TWC,i}} = 3$ (as assumed in Korolev et al., 2013) instead of 1 induces an increase of LWC by 10 % only.

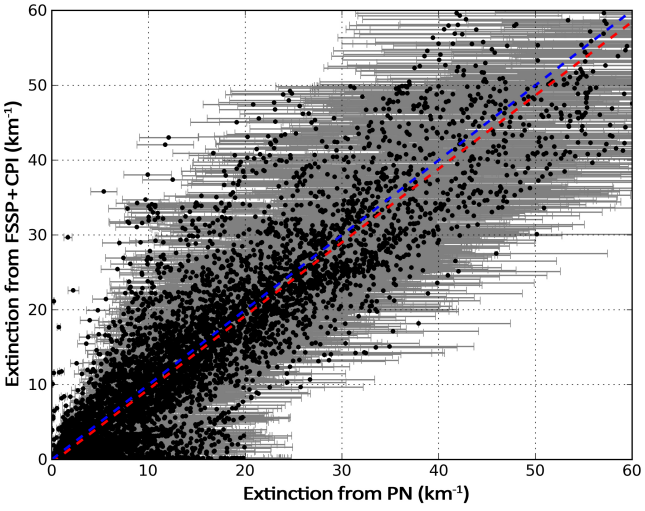

Figure B1. Comparison of extinction from PN and FSSP plus CPI measurements. Grey bars represent the 25 % uncertainties on the PN extinction. The red dotted line is the linear fitting (slope of 0.98, $R^2 = 0.87$) and the blue dotted line is the 1 : 1 line.

The uncertainties associated with the microphysical and optical properties derived from FSSP-100, PN, Nevzorov and CPI measurements are detailed in Baumgardner and Spowart (1990), Gayet et al. (2002), Korolev et al. (1998), and Mioche (2010), respectively, and are summarized in Table 2.

Appendix B: Effects of the shattering of ice crystals on measurements

Techniques and methods exist now to avoid or estimate this shattering effect, such as newly designed inlets or measurements of the particles' interarrival time (Field et al., 2003), but none of these were available for this study. However, in order to assess the accuracy of the present dataset and highlight a possible impact of the shattering effect, a brief intercomparison of the extinction coefficient from the three datasets was conducted. Indeed, the extinction coefficient is the only parameter which can be derived by the measurements of the three probes. Moreover, it is not determined with the same method, since it is calculated from the PSD for the CPI and the FSSP and from the scattering phase function for the PN. One more important point is that CPI, FSSP and PN all have different size inlets (23, 40 and 10 mm diameters, respectively). So, from this information, we could assume that, if a shattering effect is present on ice particles, its magnitude (i.e., the number of smaller new artifact particles) would differ from one instrument to another. Thus, the comparison of the extinction coefficient from CPI, FSSP and PN measurements would highlight such discrepancies.

Figure B1 displays the comparison of the extinction coefficient derived from the PN and from the combination of the CPI and FSSP for all the in situ data available for this study. Note that the combination of CPI and FSSP data covers the same size range of the PN. Figure B1 clearly shows that the extinction coefficient measurements derived from the combination of the CPI and FSSP and the PN are very well correlated (with a coefficient of 0.87) and no significant bias is observed (regression coefficient of 0.98). Thus, since the design of the instruments and data processing are different for each dataset, these results highlight that the shattering effect is probably smaller than the measurement uncertainties (25, 35 and 55 % for PN, FSSP and CPI, respectively; see Table 2).

Competing interests. The authors declare that they have no conflict of interest.

Acknowledgements. This research was funded by the Centre National de la Recherche Scientifique – Institut National des Sciences de l'Univers (CNRS-INSU) and the Expecting EarthCare Learning from A-Train (EECLAT) project. We thank the Alfred Wegener Institute (AWI) and the Service des Avions Français Instrumentés pour la Recherche en Environnement (SAFIRE) for the organization of the campaigns and for providing research aircrafts. The authors acknowledge the NOAA Air Resources Laboratory (ARL) for the provision of the HYSPLIT transport and dispersion model and READY website (http://www.arl.noaa.gov/ready.html) used in this publication. We thank Peter Tunved from the Stockholm University for providing the aerosol data from Mount Zeppelin station via the EBAS database. We thank the anonymous reviewers who made very useful comments that strengthened the manuscript.

Edited by: Martina Krämer
Reviewed by: two anonymous referees

References

Avramov, A. and Harrington, J. Y.: Influence of parameterized ice habit on simulated mixed phase Arctic clouds, J. Geophys. Res., 115, D03205, https://doi.org/10.1029/2009JD012108, 2010.

Avramov, A., Ackerman, A. S., Fridlind, A. M., van Diedenhoven, B., Botta, G., Aydin, K., Verlinde, J., Korolev, A. V., Strapp, J. W., McFarquhar, G. M., Jackson, R., Brooks, S. D., Glen, A., and Wolde, M.: Toward ice formation closure in Arctic mixed-phase boundary layer clouds during ISDAC, J. Geophys. Res., 116, D00T08, https://doi.org/10.1029/2011JD015910, 2011.

Baker, B. and Lawson, R. P.: Improvement in Determination of Ice Water Content from Two-Dimensional Particle Imagery. Part I: Image-to-Mass Relationships, J. Appl. Meteorol. Clim., 45, 1282–1290, https://doi.org/10.1175/JAM2398.1, 2006.

Baumgardner, D. and Spowart, M.: Evaluation of the Forward Scattering Spectrometer Probe. Part III: Time Response and Laser Inhomogeneity Limitations, J. Atmos. Ocean. Tech., 7, 666–672, https://doi.org/10.1175/1520-0426(1990)007<0666:EOTFSS>2.0.CO;2, 1990.

Baumgardner, D., Gayet, J.-F., Gerber, H., Korolev, A. V., and Twohy, C.: Clouds/Measurement Techniques In Situ, in: Encyclopedia of Atmospheric Sciences, in: Encyclopedia of Atmospheric Sciences, p. 4000, edited by: Holton, J. R., Curry, J. A., and Pyle, J., London, 2002.

Baumgardner, D., Avallone, L., Bansemer, A., Borrmann, S., Brown, P., Bundke, U., Chuang, P. Y., Cziczo, D., Field, P., Gallagher, M., Gayet, J.-F., Heymsfield, A., Korolev, A., Krämer, M., McFarquhar, G., Mertes, S., Möhler, O., Lance, S., Lawson, P., Petters, M. D., Pratt, K., Roberts, G., Rogers, D., Stetzer, O., Stith, J., Strapp, W., Twohy, C., and Wendisch, M.: In Situ, Airborne Instrumentation: Addressing and Solving Measurement Problems in Ice Clouds, B. Am. Meteorol. Soc., 93, ES29–ES34, https://doi.org/10.1175/BAMS-D-11-00123.1, 2012.

Baumgardner, D., Newton, R., Krämer, M., Meyer, J., Beyer, A., Wendisch, M., and Vochezer, P.: The Cloud Particle Spectrometer with Polarization Detection (CPSPD): A next generation open-path cloud probe for distinguishing liquid cloud droplets from ice crystals, Atmos. Res., 142, 2–14, https://doi.org/10.1016/j.atmosres.2013.12.010, 2014.

Bergeron, T.: On the physics of clouds and precipitation, Proces Verbaux de l'Association de Météorologie, International Union of Geodesy and Geophysics, 156–178, 1935.

Bierwirth, E., Ehrlich, A., Wendisch, M., Gayet, J.-F., Gourbeyre, C., Dupuy, R., Herber, A., Neuber, R., and Lampert, A.: Optical thickness and effective radius of Arctic boundary-layer clouds retrieved from airborne nadir and imaging spectrometry, Atmos. Meas. Tech., 6, 1189–1200, https://doi.org/10.5194/amt-6-1189-2013, 2013.

Cober, S. G., Isaac, G. A., Korolev, A. V., and Strapp, J. W.: Assessing Cloud-Phase Conditions, J. Appl. Meteorol., 40, 1967–1983, https://doi.org/10.1175/1520-0450(2001)040<1967:ACPC>2.0.CO;2, 2001.

Cooper, W. A.: Ice Initiation in Natural Clouds, Meteor. Mon., 21, 29–32, https://doi.org/10.1175/0065-9401-21.43.29, 1986.

Curry, J. A.: Interactions among aerosols, clouds, and climate of the Arctic Ocean, Sci. Total Environ., 160–161, 777–791, https://doi.org/10.1016/0048-9697(95)04411-S, 1995.

Curry, J. A., Schramm, J. L., Rossow, W. B., and Randall, D.: Overview of Arctic Cloud and Radiation Characteristics, J. Climate, 9, 1731–1764, https://doi.org/10.1175/1520-0442(1996)009<1731:OOACAR>2.0.CO;2, 1996.

de Boer, G., Eloranta, E. W., and Shupe, M. D.: Arctic Mixed-Phase Stratiform Cloud Properties from Multiple Years of Surface-Based Measurements at Two High-Latitude Locations, J. Atmos. Sci., 66, 2874–2887, https://doi.org/10.1175/2009JAS3029.1, 2009.

Delanoë, J., Protat, A., Jourdan, O., Pelon, J., Papazzoni, M., Dupuy, R., Gayet, J.-F., and Jouan, C.: Comparison of Airborne In Situ, Airborne Radar–Lidar, and Spaceborne Radar–Lidar Retrievals of Polar Ice Cloud Properties Sampled during the POLARCAT Campaign, J. Atmos. Ocean. Tech., 30, 57–73, https://doi.org/10.1175/JTECH-D-11-00200.1, 2013.

DeMott, P. J., Möhler, O., Stetzer, O., Vali, G., Levin, Z., Petters, M. D., Murakami, M., Leisner, T., Bundke, U., Klein, H., Kanji, Z. A., Cotton, R., Jones, H., Benz, S., Brinkmann, M., Rzesanke, D., Saathoff, H., Nicolet, M., Saito, A., Nillius, B., Bingemer, H., Abbatt, J., Ardon, K., Ganor, E., Georgakopoulos, D. G., and Saunders, C.: Resurgence in Ice Nuclei Measurement Research, B. Am. Meteorol. Soc., 92, 1623–1635, https://doi.org/10.1175/2011BAMS3119.1, 2011.

Dong, X., Xi, B., Crosby, K., Long, C. N., Stone, R. S., and Shupe, M. D.: A 10 year climatology of Arctic cloud fraction and radiative forcing at Barrow, Alaska, J. Geophys. Res., 115, D17212, https://doi.org/10.1029/2009JD013489, 2010.

Stein, A. F., Draxler, R. R, Rolph, G. D., Stunder, B. J. B., Cohen, M. D., and Ngan, F.: NOAA's HYSPLIT atmospheric transport and dispersion modeling system, B. Am. Meteorol. Soc., 96, 2059–2077, https://doi.org/10.1175/BAMS-D-14-00110.1, 2015.

Ehrlich, A., Wendisch, M., Bierwirth, E., Gayet, J.-F., Mioche, G., Lampert, A., and Mayer, B.: Evidence of ice crystals at cloud top of Arctic boundary-layer mixed-phase clouds derived from airborne remote sensing, Atmos. Chem. Phys., 9, 9401–9416, https://doi.org/10.5194/acp-9-9401-2009, 2009.

Eidhammer, T., DeMott, P. J., Prenni, A. J., Petters, M. D., Twohy, C. H., Rogers, D. C., Stith, J., Heymsfield, A., Wang, Z., Pratt, K. A., Prather, K. A., Murphy, S. M., Seinfeld, J. H., Subramanian, R., and Kreidenweis, S. M.: Ice Initiation by Aerosol Particles: Measured and Predicted Ice Nuclei Concentrations versus Measured Ice Crystal Concentrations in an Orographic Wave Cloud, J. Atmos. Sci., 67, 2417–2436, https://doi.org/10.1175/2010JAS3266.1, 2010.

Febvre, G., Gayet, J.-F., Shcherbakov, V., Gourbeyre, C., and Jourdan, O.: Some effects of ice crystals on the FSSP measurements in mixed phase clouds, Atmos. Chem. Phys., 12, 8963–8977, https://doi.org/10.5194/acp-12-8963-2012, 2012.

Field, P. R., Wood, R., Brown, P. R. A., Kaye, P. H., Hirst, E., Greenaway, R., and Smith, J. A.: Ice Particle Interarrival Times Measured with a Fast FSSP, J. Atmos. Ocean. Tech., 20, 249–261, https://doi.org/10.1175/1520-0426(2003)020<0249:IPITMW>2.0.CO;2, 2003.

Findeisen, W.: Kolloid-meteorologische vorgange bei neiderschlags-bildung, Meteorol. Z., 55, 121–133, 1938.

Fridlind, A. M., Ackerman, A. S., McFarquhar, G., Zhang, G., Poellot, M. R., DeMott, P. J., Prenni, A. J., and Heymsfield, A. J.: Ice properties of single-layer stratocumulus during the Mixed-Phase Arctic Cloud Experiment: 2. Model results, J. Geophys. Res., 112, D24, https://doi.org/10.1029/2007JD008646, 2007.

Gayet, J. F., Crépel, O., Fournol, J. F., and Oshchepkov, S.: A new airborne polar Nephelometer for the measurements of optical and microphysical cloud properties. Part I: Theoretical design, Ann. Geophys., 15, 451–459, https://doi.org/10.1007/s00585-997-0451-1, 1997.

Gayet, J.-F., Asano, S., Yamazaki, A., Uchiyama, A., Sinyul, A., Jourdan, O., and Auriol, F.: Two case studies of winter continental-type water and mixed-phase stratocumuli over the sea 1. Microphysical and optical properties, J. Geophys. Res., 107, D21, https://doi.org/10.1029/2001JD001106, 2002.

Gayet, J.-F., Mioche, G., Dörnbrack, A., Ehrlich, A., Lampert, A., and Wendisch, M.: Microphysical and optical properties of Arctic mixed-phase clouds. The 9 April 2007 case study., Atmos. Chem. Phys., 9, 6581–6595, https://doi.org/10.5194/acp-9-6581-2009, 2009.

Gerber, H., Takano, Y., Garrett, T. J., and Hobbs, P. V.: Nephelometer measurements of the asymmetry parameter, volume extinction coefficient and backscatter ratio in Artic clouds, J. Atmos. Sci., 57, 3021–3034, 2000.

Gultepe, I. and Isaac, G. A.: Effects of air mass origin on Arctic cloud microphysical parameters for April 1998 during FIRE.ACE, J. Geophys. Res., 107, D21, https://doi.org/10.1029/2000JC000440, 2002.

Gultepe, I., Isaac, G., Hudak, D., Nissen, R., and Strapp, J. W.: Dynamical and Microphysical Characteristics of Arctic Clouds during BASE, J. Climate, 13, 1225–1254, https://doi.org/10.1175/1520-0442(2000)013<1225:DAMCOA>2.0.CO;2, 2000.

Guyot, G., Gourbeyre, C., Febvre, G., Shcherbakov, V., Burnet, F., Dupont, J.-C., Sellegri, K., and Jourdan, O.: Quantitative evaluation of seven optical sensors for cloud microphysical measurements at the Puy-de-Dôme Observatory, France, Atmos. Meas. Tech., 8, 4347–4367, https://doi.org/10.5194/amt-8-4347-2015, 2015.

Herber, A., Gayet, J.-F., Hara, K., Krecji, R., Minikin, A., Neuber, R., Ritter, C., Schrems, O., Ström, J., Schwarzenboeck, A., Treffeisen, R., Yamagata, S., and Yamanouchi, T.: Arctic Study of Troposheric Aerosols, Clouds and Radiation, ASTAR 2004: First Results, Budapest, Hungary, 2004.

Heymsfield, A. J.: On measurements of small ice particles in clouds: Small particles in ice clouds, Geophys. Res. Lett., 34, 10, https://doi.org/10.1029/2007GL030951, 2007.

Heymsfield, A. J., Winker, D., and Zadelhoff, G.-J.: Extinction-ice water content-effective radius algorithms for CALIPSO, Geophys. Res. Lett., 32, 10, https://doi.org/10.1029/2005GL022742, 2005.

Hobbs, P. V., Rangno, A. L., Shupe, M., and Uttal, T.: Airborne studies of cloud structures over the Arctic Ocean and comparisons with retrievals from ship-based remote sensing measurements, J. Geophys. Res., 106, 15029, https://doi.org/10.1029/2000JD900323, 2001.

Hogan, R. J., Mittermaier, M. P., and Illingworth, A. J.: The Retrieval of Ice Water Content from Radar Reflectivity Factor and Temperature and Its Use in Evaluating a Mesoscale Model, J. Appl. Meteorol. Clim., 45, 301–317, https://doi.org/10.1175/JAM2340.1, 2006.

Jackson, R. C., McFarquhar, G. M., Korolev, A. V., Earle, M. E., Liu, P. S. K., Lawson, R. P., Brooks, S., Wolde, M., Laskin, A., and Freer, M.: The dependence of ice microphysics on aerosol concentration in Arctic mixed-phase stratus clouds during ISDAC and M-PACE, J. Geophys. Res., 117, D15207, https://doi.org/10.1029/2012JD017668, 2012.

Jourdan, O., Mioche, G., Garrett, T. J., Schwarzenböck, A., Vidot, J., Xie, Y., Shcherbakov, V., Yang, P., and Gayet, J.-F.: Coupling of the microphysical and optical properties of an Arctic nimbostratus cloud during the ASTAR 2004 experiment: Implications for light-scattering modeling, J. Geophys. Res., 115, D23206, https://doi.org/10.1029/2010JD014016, 2010.

Kay, J. E. and Gettelman, A.: Cloud influence on and response to seasonal Arctic sea ice loss, J. Geophys. Res., 114, D18204, https://doi.org/10.1029/2009JD011773, 2009.

Kay, J. E., Holland, M. M., Bitz, C. M., Blanchard-Wrigglesworth, E., Gettelman, A., Conley, A., and Bailey, D.: The Influence of Local Feedbacks and Northward Heat Transport on the Equilibrium Arctic Climate Response to Increased Greenhouse Gas Forcing, J. Climate, 25, 5433–5450, https://doi.org/10.1175/JCLI-D-11-00622.1, 2012.

Klein, S. A., McCoy, R. B., Morrison, H., Ackerman, A. S., Avramov, A., Boer, G. de, Chen, M., Cole, J. N. S., Del Genio, A. D., Falk, M., Foster, M. J., Fridlind, A., Golaz, J.-C., Hashino, T., Harrington, J. Y., Hoose, C., Khairoutdinov, M. F., Larson, V. E., Liu, X., Luo, Y., McFarquhar, G. M., Menon, S., Neggers, R. A. J., Park, S., Poellot, M. R., Schmidt, J. M., Sednev, I., Shipway, B. J., Shupe, M. D., Spangenberg, D. A., Sud, Y. C., Turner, D. D., Veron, D. E., Salzen, K. von, Walker, G. K., Wang, Z., Wolf, A. B., Xie, S., Xu, K.-M., Yang, F., and Zhang, G.: Intercomparison of model simulations of mixed-phase clouds observed during the ARM Mixed-Phase Arctic Cloud Experiment. I: single-layer cloud, Q. J. Roy. Meteor. Soc., 135, 979–1002, https://doi.org/10.1002/qj.416, 2009.

Knollenberg, R. G.: Techniques for probing cloud microstructure, in: Clouds, Their Formation, Optical Properties, and Effects, edited by: Hobbs, P. V. and Deepak, A., New-York, 5–91, 1981.

Komurcu, M., Storelvmo, T., Tan, I., Lohmann, U., Yun, Y., Penner, J. E., Wang, Y., Liu, X., and Takemura, T.: INter-comparison of the cloud water phase among global climate models: cloud water phase in GCMs, J. Geophys. Res.-Atmos., 119, 3372–3400, https://doi.org/10.1002/2013JD021119, 2014.

Korolev, A.: Limitations of the Wegener–Bergeron–Findeisen Mechanism in the Evolution of Mixed-Phase Clouds, J. Atmos. Sci., 64, 3372–3375, https://doi.org/10.1175/JAS4035.1, 2007.

Korolev, A. and Isaac, G.: Phase transformation of mixed-phase clouds, Q. J. Roy. Meteor. Soc., 129, 19–38, https://doi.org/10.1256/qj.01.203, 2003.

Korolev, A. V., Strapp, J. W., Isaac, G. A., and Nevzorov, A. N.: The Nevzorov Airborne Hot-Wire LWC–TWC Probe: Principle of Operation and Performance Characteristics, J. Atmos. Ocean. Tech., 15, 1495–1510, https://doi.org/10.1175/1520-0426(1998)015<1495:TNAHWL>2.0.CO;2, 1998.

Korolev, A. V., Isaac, G. A., and Hallett, J.: Ice particle habits in Arctic clouds, Geophys. Res. Lett., 26, 1299–1302, 1999.

Korolev, A. V., Isaac, G. A., Cober, S. G., Strapp, J. W., and Hallett, J.: Microphysical characterization of mixed-phase clouds, Q. J. Roy. Meteor. Soc., 129, 39–65, https://doi.org/10.1256/qj.01.204, 2003.

Korolev, A. V., Emery, E. F., Strapp, J. W., Cober, S. G., Isaac, G. A., Wasey, M., and Marcotte, D.: Small Ice Particles in Tropospheric Clouds: Fact or Artifact? Airborne Icing Instrumentation Evaluation Experiment, B. Am. Meteorol. Soc., 92, 967–973, https://doi.org/10.1175/2010BAMS3141.1, 2011.

Korolev, A. V., Emery, E. F., Strapp, J. W., Cober, S. G., and Isaac, G. A.: Quantification of the Effects of Shattering on Airborne Ice Particle Measurements, J. Atmos. Ocean. Tech., 30, 2527–2553, https://doi.org/10.1175/JTECH-D-13-00115.1, 2013.

Lampert, A., Ehrlich, A., Dörnbrack, A., Jourdan, O., Gayet, J.-F., Mioche, G., Shcherbakov, V., Ritter, C., and Wendisch, M.: Microphysical and radiative characterization of a subvisible mid-level Arctic ice cloud by airborne observations – a case study, Atmos. Chem. Phys., 9, 2647–2661, https://doi.org/10.5194/acp-9-2647-2009, 2009.

Lance, S., Shupe, M. D., Feingold, G., Brock, C. A., Cozic, J., Holloway, J. S., Moore, R. H., Nenes, A., Schwarz, J. P., Spackman, J. R., Froyd, K. D., Murphy, D. M., Brioude, J., Cooper, O. R., Stohl, A., and Burkhart, J. F.: Cloud condensation nuclei as a modulator of ice processes in Arctic mixed-phase clouds, Atmos. Chem. Phys., 11, 8003–8015, https://doi.org/10.5194/acp-11-8003-2011, 2011.

Law, K. S., Ancellet, G., Pelon, J., Turquety, S., Clerbaux, C., Pommier, M., de Villiers, R., Gayet, J.-F., Schwarzenboeck, A., Nedelec, P., Schneider, J., and Borrmann, S.: POLARCAT-France Airborne Experiment: first results, Annecy, France, 7–12, 2008.

Lawson, R. P. and Baker, B. A.: Improvement in Determination of Ice Water Content from Two-Dimensional Particle Imagery. Part II: Applications to Collected Data, J. Appl. Meteorol. Clim., 45, 1291–1303, https://doi.org/10.1175/JAM2399.1, 2006.

Lawson, R. P., Baker, B. A., Schmitt, C. G., and Jensen, T. L.: An overview of microphysical properties of Arctic clouds observed in May and July 1998 during FIRE ACE, J. Geophys. Res., 106, 14989, https://doi.org/10.1029/2000JD900789, 2001.

Lefèvre, R.: Physique de la mesure de la sonde CPI pour la mesure des propriétés des cristaux de glace. Application aux observations réalisées durant la campagne ASTAR 2004, Université Blaise Pascal, Aubière, France, 2007.

Libbrecht, K. G.: The physics of snow crystals, Rep. Prog. Phys., 68, 855–895, https://doi.org/10.1088/0034-4885/68/4/R03, 2005.

Liu, Y., Key, J. R., Ackerman, S. A., Mace, G. G., and Zhang, Q.: Arctic cloud macrophysical characteristics from CloudSat and CALIPSO, Remote Sens. Environ., 124, 159–173, https://doi.org/10.1016/j.rse.2012.05.006, 2012.

Lloyd, G., Choularton, T. W., Bower, K. N., Crosier, J., Jones, H., Dorsey, J. R., Gallagher, M. W., Connolly, P., Kirchgaessner, A. C. R., and Lachlan-Cope, T.: Observations and comparisons of cloud microphysical properties in spring and summertime Arctic stratocumulus clouds during the ACCACIA campaign, Atmos. Chem. Phys., 15, 3719–3737, https://doi.org/10.5194/acp-15-3719-2015, 2015.

McFarquhar, G. M., Zhang, G., Poellot, M. R., Kok, G. L., McCoy, R., Tooman, T., Fridlind, A., and Heymsfield, A. J.: Ice properties of single-layer stratocumulus during the Mixed-Phase Arctic Cloud Experiment: 1. Observations, J. Geophys. Res., 112, 24201, https://doi.org/10.1029/2007JD008633, 2007.

McFarquhar, G. M., Ghan, S., Verlinde, J., Korolev, A., Strapp, J. W., Schmid, B., Tomlinson, J. M., Wolde, M., Brooks, S. D., Cziczo, D., Dubey, M. K., Fan, J., Flynn, C., Gultepe, I., Hubbe, J., Gilles, M. K., Laskin, A., Lawson, P., Leaitch, W. R., Liu, P., Liu, X., Lubin, D., Mazzoleni, C., Macdonald, A.-M., Moffet, R. C., Morrison, H., Ovchinnikov, M., Shupe, M. D., Turner, D. D., Xie, S., Zelenyuk, A., Bae, K., Freer, M., and Glen, A.: Indirect and Semi-direct Aerosol Campaign: The Impact of Arctic Aerosols on Clouds, B. Am. Meteorol. Soc., 92, 183–201, https://doi.org/10.1175/2010BAMS2935.1, 2011.

Meyers, M. P., DeMott, P. J., and Cotton, W. R.: New Primary Ice-Nucleation Parameterizations in an Explicit Cloud Model, J. Appl. Meteorol., 31, 708–721, https://doi.org/10.1175/1520-0450(1992)031<0708:NPINPI>2.0.CO;2, 1992.

Mioche, G.: Validation des produits d'inversion des observations satellitaires CALIPSO et CloudSat pour la caractérisation des propriétés optiques et microphysiques des nuages de glace et en phase mixte, Université Blaise Pascal, Aubière, France, 2010.

Mioche, G., Jourdan, O., Ceccaldi, M., and Delanoë, J.: Variability of mixed-phase clouds in the Arctic with a focus on the Svalbard region: a study based on spaceborne active remote sensing, Atmos. Chem. Phys., 15, 2445–2461, https://doi.org/10.5194/acp-15-2445-2015, 2015.

Morrison, H. and Pinto, J. O.: Intercomparison of Bulk Cloud Microphysics Schemes in Mesoscale Simulations of Springtime Arctic Mixed-Phase Stratiform Clouds, Mon. Weather Rev., 134, 1880–1900, https://doi.org/10.1175/MWR3154.1, 2006.

Morrison, H., de Boer, G., Feingold, G., Harrington, J., Shupe, M. D., and Sulia, K.: Resilience of persistent Arctic mixed-phase clouds, Nat. Geosci., 5, 11–17, https://doi.org/10.1038/ngeo1332, 2012.

Nakaya, U.: Snow Crystals: Natural and Artificial, Cambridge Harvard University Press, 1954.

Ovchinnikov, M., Ackerman, A. S., Avramov, A., Cheng, A., Fan, J., Fridlind, A. M., Ghan, S., Harrington, J., Hoose, C., Korolev, A., McFarquhar, G. M., Morrison, H., Paukert, M., Savre, J., Shipway, B. J., Shupe, M. D., Solomon, A., and Sulia, K.: Intercomparison of large-eddy simulations of

Arctic mixed-phase clouds: Importance of ice size distribution assumptions, J. Adv. Model. Earth Syst., 6, 223–248, https://doi.org/10.1002/2013MS000282, 2014.

Pinto, J. O.: Autumnal Mixed-Phase Cloudy Boundary Layers in the Arctic, J. Atmos. Sci., 55, 2016–2038, https://doi.org/10.1175/1520-0469(1998)055<2016:AMPCBL>2.0.CO;2, 1998.

Pinto, J. O. and Curry, J. A.: Cloud-aerosol interactions during autumn over Beaufort Sea, J. Geophys. Res., 106, 15077–15097, 2001.

Prenni, A. J., DeMott, P. J., Kreidenweis, S. M., Harrington, J. Y., Avramov, A., Verlinde, J., Tjernström, M., Long, C. N., and Olsson, P. Q.: Can Ice-Nucleating Aerosols Affect Arctic Seasonal Climate?, B. Am. Meteorol. Soc., 88, 541–550, https://doi.org/10.1175/BAMS-88-4-541, 2007.

Prenni, A. J., Demott, P. J., Rogers, D. C., Kreidenweis, S. M., Mcfarquhar, G. M., Zhang, G., and Poellot, M. R.: Ice nuclei characteristics from M-PACE and their relation to ice formation in clouds, Tellus B, 61, 436–448, https://doi.org/10.1111/j.1600-0889.2009.00415.x, 2009.

Protat, A., Delanoë, J., Bouniol, D., Heymsfield, A. J., Bansemer, A., and Brown, P.: Evaluation of Ice Water Content Retrievals from Cloud Radar Reflectivity and Temperature Using a Large Airborne In Situ Microphysical Database, J. Appl. Meteorol. Clim., 46, 557–572, https://doi.org/10.1175/JAM2488.1, 2007.

Protat, A., Delanoë, J., Strapp, J. W., Fontaine, E., Leroy, D., Schwarzenboeck, A., Lilie, L., Davison, C., Dezitter, F., Grandin, A., and Weber, M.: The Measured Relationship between Ice Water Content and Cloud Radar Reflectivity in Tropical Convective Clouds, J. Appl. Meteorol. Clim., 55, 1707–1729, https://doi.org/10.1175/JAMC-D-15-0248.1, 2016.

Pruppacher, H. R. and Klett, J. D.: Microphysics of Clouds and Precipitation, Springer Netherlands, Dordrecht, available at: http://link.springer.com/10.1007/978-94-009-9905-3 (last access: 22 December 2015), 1978.

Quennehen, B., Schwarzenboeck, A., Schmale, J., Schneider, J., Sodemann, H., Stohl, A., Ancellet, G., Crumeyrolle, S., and Law, K. S.: Physical and chemical properties of pollution aerosol particles transported from North America to Greenland as measured during the POLARCAT summer campaign, Atmos. Chem. Phys., 11, 10947–10963, https://doi.org/10.5194/acp-11-10947-2011, 2011.

Rangno, A. L. and Hobbs, P. V.: Ice particles in stratiform clouds in the Arctic and possible mechanisms for the production of high ice concentrations, J. Geophys. Res., 106, 15065, https://doi.org/10.1029/2000JD900286, 2001.

Savre, J. and Ekman, A. M. L.: Large-eddy simulation of three mixed-phase cloud events during ISDAC: Conditions for persistent heterogeneous ice formation: LES OF ICE NUCLEATION DURING ISDAC, J. Geophys. Res.-Atmos., 120, 7699–7725, https://doi.org/10.1002/2014JD023006, 2015.

Schwarzenboeck, A., Mioche, G., Armetta, A., Herber, A., and Gayet, J.-F.: Response of the Nevzorov hot wire probe in clouds dominated by droplet conditions in the drizzle size range, Atmos. Meas. Tech., 2, 779–788, https://doi.org/10.5194/amt-2-779-2009, 2009.

Shupe, M. D. and Intrieri, J. M.: Cloud Radiative Forcing of the Arctic Surface: The Influence of Cloud Properties, Surface Albedo, and Solar Zenith Angle, J. Climate, 1, 616–628, https://doi.org/10.1175/1520-0442(2004)017<0616:CRFOTA>2.0.CO;2, 2004.

Shupe, M. D., Matrosov, S. Y., and Uttal, T.: Arctic Mixed-Phase Cloud Properties Derived from Surface-Based Sensors at SHEBA, J. Atmos. Sci., 63, 697–711, https://doi.org/10.1175/JAS3659.1, 2006.

Shupe, M. D., Daniel, J. S., de Boer, G., Eloranta, E. W., Kollias, P., Luke, E. P., Long, C. N., Turner, D. D., and Verlinde, J.: A Focus On Mixed-Phase Clouds: The Status of Ground-Based Observational Methods, B. Am. Meteorol. Soc., 89, 1549–1562, https://doi.org/10.1175/2008BAMS2378.1, 2008.

Shupe, M. D., Walden, V. P., Eloranta, E., Uttal, T., Campbell, J. R., Starkweather, S. M., and Shiobara, M.: Clouds at Arctic Atmospheric Observatories. Part I: Occurrence and Macrophysical Properties, J. Appl. Meteorol. Clim., 50, 626–644, https://doi.org/10.1175/2010JAMC2467.1, 2011.

Solomon, A., Feingold, G., and Shupe, M. D.: The role of ice nuclei recycling in the maintenance of cloud ice in Arctic mixed-phase stratocumulus, Atmos. Chem. Phys., 15, 10631–10643, https://doi.org/10.5194/acp-15-10631-2015, 2015.

Solomon, S., Qin, D., Manning, M., Chen, Z., Marquis, M., Averyt, K. B., Tignor, M., and Miller, H. L.: Climate change 2007: the physical scence basis, Cambridge University Press, Cambridge, UK, 2007.

Stephens, G. L., Vane, D. G., Boain, R. J., Mace, G. G., Sassen, K., Wang, Z., Illingworth, A. J., O'Connor, E. J., Rossow, W. B., Durden, S. L., Miller, S. D., Austin, R. T., Benedetti, A., Mitrescu, C., and CloudSat Science Team, T.: The CloudSat mission and the A-Train: a new dimension of space-based observations of clouds and precipitation, B. Am. Meteorol. Soc., 83, 1771–1790, https://doi.org/10.1175/BAMS-83-12-1771, 2002.

Tan, I. and Storelvmo, T.: Sensitivity Study on the Influence of Cloud Microphysical Parameters on Mixed-Phase Cloud Thermodynamic Phase Partitioning in CAM5, J. Atmos. Sci., 73, 709–728, https://doi.org/10.1175/JAS-D-15-0152.1, 2016.

Ulanowski, Z., Kaye, P. H., Hirst, E., Greenaway, R. S., Cotton, R. J., Hesse, E., and Collier, C. T.: Incidence of rough and irregular atmospheric ice particles from Small Ice Detector 3 measurements, Atmos. Chem. Phys., 14, 1649–1662, https://doi.org/10.5194/acp-14-1649-2014, 2014.

Verlinde, J., Harrington, J. Y., Yannuzzi, V. T., Avramov, A., Greenberg, S., Richardson, S. J., Bahrmann, C. P., McFarquhar, G. M., Zhang, G., Johnson, N., Poellot, M. R., Mather, J. H., Turner, D. D., Eloranta, E. W., Tobin, D. C., Holz, R., Zak, B. D., Ivey, M. D., Prenni, A. J., DeMott, P. J., Daniel, J. S., Kok, G. L., Sassen, K., Spangenberg, D., Minnis, P., Tooman, T. P., Shupe, M., Heymsfield, A. J., and Schofield, R.: The Mixed-Phase Arctic Cloud Experiment, B. Am. Meteorol. Soc., 88, 205–221, https://doi.org/10.1175/BAMS-88-2-205, 2007.

Vochezer, P., Järvinen, E., Wagner, R., Kupiszewski, P., Leisner, T., and Schnaiter, M.: In situ characterization of mixed phase clouds using the Small Ice Detector and the Particle Phase Discriminator, Atmos. Meas. Tech., 9, 159–177, https://doi.org/10.5194/amt-9-159-2016, 2016.

Waliser, D. E., Li, J.-L. F., Woods, C. P., Austin, R. T., Bacmeister, J., Chern, J., Del Genio, A., Jiang, J. H., Kuang, Z., Meng, H., Minnis, P., Platnick, S., Rossow, W. B., Stephens, G. L., Sun-Mack, S., Tao, W.-K., Tompkins, A. M., Vane, D. G., Walker, C., and Wu, D.: Cloud ice: A climate model challenge with

signs and expectations of progress, J. Geophys. Res., 114, D8, https://doi.org/10.1029/2008JD010015, 2009.

Wegener, A.: Thermodynamik der Atmosphare, J. A. Barth, Leipzig, 1911.

Winker, D. M., Pelon, J. R., and McCormick, M. P.: The CALIPSO mission: spaceborne lidar for observation of aerosols and clouds, 4893, 1–11, Proceedings of SPIE, 4893, Hangzhou, China, 2003.

Young, G., Connolly, P. J., Jones, H. M., and Choularton, T. W.: Microphysical sensitivity of coupled springtime Arctic stratocumulus to modelled primary ice over the ice pack, marginal ice, and ocean, Atmos. Chem. Phys., 17, 4209–4227, https://doi.org/10.5194/acp-17-4209-2017, 2017.